



Temporal evolution of shallow marine diagenetic environments: Insights from carbonate concretions

Sean J. Loyd^{a,*}, Patrick Meister^b, Bo Liu^c, Kevin Nichols^d, Frank A. Corsetti^e, Robert Raiswell^f, William Berelson^e, Graham Shields^g, Mark Hounslow^{h,i}, John W.F. Waldron^j, Bayne Westrick-Snapp^a, Jamie Hoffman^a

^a Department of Geological Sciences, California State University, Fullerton, Fullerton, CA 92831, United States

^b Department of Geology, University of Vienna, Vienna, Austria

^c Alfred-Wegener Institute Helmholtz Centre for Polar and Marine Research, Bremerhaven, Germany

^d Department of Mathematics, California State University, Fullerton, Fullerton, CA 92831, United States

^e Department of Earth Sciences, University of Southern California, Los Angeles, CA 90089, United States

^f School of Earth and Environment, University of Leeds, Leeds LS2 9JT, United Kingdom

^g Department of Earth Sciences, University College London, London WC1E 6BT, United Kingdom

^h CEMP, Geography Department, Lancaster Environment Centre, Lancaster University, Lancaster LA1 4YW, United Kingdom

ⁱ Department of Earth, Ocean and Ecological Sciences, University of Liverpool, Liverpool L69 3GP, United Kingdom

^j Department of Earth and Atmospheric Sciences, University of Alberta, Edmonton, AB T6G 2E3, Canada

ARTICLE INFO

Associate editor: Noah J. Planavsky

Keywords:

Carbonate concretion

Organic carbon

Sulfate

Methanogenesis

Anaerobic oxidation of methane (AOM)

Authigenic carbonate

ABSTRACT

Early diagenesis of marine organic matter dramatically impacts Earth's surface chemistry by changing the burial potential of carbon and promoting the formation of authigenic mineral phases including carbonate concretions. Marine sediment-hosted carbonate concretions tend to form as a result of microbial anaerobic diagenetic reactions that degrade organic matter and methane, some of which require an external oxidant. Thus, temporal changes in the oxidation state of Earth's oceans may impart a first-order control on concretion authigenesis mechanisms through time. Statistically significant variability in concretion carbonate carbon isotope compositions indicates changes in shallow marine sediment diagenesis associated with Earth's evolving redox landscape. This variability manifests itself as an expansion in carbon isotope composition range broadly characterized by an increase in maximum and decrease in minimum isotope values through time. Reaction transport modelling helps to constrain the potential impacts of shifting redox chemistry and highlights the importance of organic carbon delivery to the seafloor, marine sulfate concentrations, methane production and external methane influx. The first appearance of conclusively anaerobic oxidation of methane-derived concretions occurs in the Carboniferous and coincides with a Paleozoic rise in marine sulfate. The muted variability recognized in older concretions (and in particular for Precambrian concretions) likely reflects impacts of a smaller marine sulfate reservoir and perhaps elevated marine dissolved inorganic carbon concentrations. Causes of the increase in carbon isotope maximum values through time are more confounding, but may be related to isotopic equilibration of dissolved inorganic carbon with externally derived methane. Ultimately the concretion isotope record in part reflects changes in organic matter availability and marine oxidation state, highlighting connections with the subsurface biosphere and diagenesis throughout geologic time.

1. Introduction

Carbonate concretions are isolated zones of relatively high cement content in sediments and sedimentary rocks (Coleman, 1993). These precipitates can exhibit textural and compositional characteristics that

indicate initial formation within shallow sediments. Shallow formation indicators include deflection of external lamination (Raiswell, 1971), preservation of delicate primary sedimentary features (such as thin walled shells and macrofauna carcasses) (Allison and Pye, 1994; Blome and Albert, 1985; Bramlette, 1946; El Albani et al., 2001; Heimhofer

* Corresponding author.

E-mail address: sloyd@fullerton.edu (S.J. Loyd).

<https://doi.org/10.1016/j.gca.2023.04.022>

Received 18 October 2022; Accepted 24 April 2023

Available online 1 May 2023

0016-7037/© 2023 The Author(s). Published by Elsevier Ltd. This is an open access article under the CC BY license (<http://creativecommons.org/licenses/by/4.0/>).

et al., 2017; Martill, 1988), evidence of biological interaction by burrowing organisms (Bjørlykke, 1973; Hesselbo and Palmer, 1992; Savrda and Bottjer, 1988), erosional exhumation (Hesselbo and Palmer, 1992) and low proxy-based formation temperatures (Dale et al., 2014; Loyd et al., 2012). Therefore, carbonate concretions can result (at least initially) from relatively shallow diagenetic processes that are intimately related to the chemical composition of marine bottom waters and the availability of organic matter delivered to the sediment–water interface. The geochemistry of Earth’s marine environments has experienced significant temporal variability in part associated with an overall increase in oxidation state (Lyons et al., 2014), associated fluctuations in marine chemistry (Canfield, 1998) and changes in organic carbon export (Krause et al., 2022; Krissansen-Totton et al., 2021; Planavsky et al., 2022) and organic matter composition (Brocks et al., 2017). In particular, variable organic carbon delivery to the seafloor and marine oxidant abundances (see below) likely impacted shallow diagenetic processes related to remineralization.

Marine sediment-hosted carbonate concretions seem to form in association with reactions that involve the microbial degradation of particulate organic matter and/or methane (Irwin et al., 1977). Of these reactions, those considered most important for concretion formation are iron reduction, organotrophic sulfate reduction, methanogenesis and the anaerobic oxidation of methane (AOM) (Claypool and Kaplan, 1974; Coleman, 1993; Irwin et al., 1977; Orphan et al., 2004). The carbon isotope composition of porewater DIC ($\delta^{13}\text{C}_{\text{DIC}}$) is impacted by the relative contributions of these pathways wherein organic matter and methane oxidation reactions cause porewater $^{13}\text{C}_{\text{DIC}}$ depletion and methanogenesis causes porewater $^{13}\text{C}_{\text{DIC}}$ enrichment. The magnitude of isotope enrichments and depletions is dictated by oxidant supply and reduced carbon source (organic matter or methane), among other factors (e.g., Meister et al., 2019). Carbonate concretions inherit the carbon isotope composition of porewater DIC owing to minimal isotope fractionation during carbonate precipitation (Emrich et al., 1970; Ohmoto and Rye, 1979). Thus, concretion carbon isotope compositions and can be used to track carbon-phase reactants (organic matter or methane) and/or reaction pathways of shallow marine diagenetic environments through time.

Here, carbonate concretion abundance and carbon isotope data (consisting of both new and previously reported data) are used to characterize ancient marine shallow diagenetic environments. These data are assessed through a transient reaction transport model to explore potential impacts of contemporaneous environmental changes. Ultimately, we show that amplified variability in concretion carbon isotope signatures coincides with proposed increases in organic carbon export and marine sulfate concentrations, implicating these factors as important for diagenetic carbonate mineralization throughout geologic time. Modeling results suggest that external methane inputs are likely required to generate severe ^{13}C depletions in concretionary carbonate. Elevated marine dissolved inorganic carbon (DIC) contents may also play a role by muting porewater isotope variability during much of the Precambrian. In addition, we identify potentially counterintuitive coincident changes in methanogenesis-driven diagenesis during the Phanerozoic.

2. Methods

Marine sediment-hosted carbonate concretion occurrence and carbonate carbon isotope composition ($\delta^{13}\text{C}_{\text{con}}$) data (~5,000 data points from ~170 units) were primarily compiled from published reports. New $\delta^{13}\text{C}_{\text{con}}$ data were collected from select time periods where isotope data have not been reported (see Supplementary Tables 1, 2). Host rock formation name, age, and lithology, and concretion mineralogy, crystallographic habit (for septarian concretions), carbon and oxygen isotope data were also collected (Supplementary Tables 1, 2 and 3), as available. Similar information provided for authigenic carbonates recovered from siliciclastic marine sediments is provided for comparison

(Supplementary Table 4). Most new concretion data were generated from powders of slabbed samples using a Dremel® rotary tool fitted with a 3-mm carbide drill bit. Triplicate 5–7 mg splits of concretion powders were dissolved in 10% phosphoric acid in sealed and evacuated ex-tainer vials. The carbon isotope composition of produced CO_2 was determined using a G2121-i Picarro® Cavity Ringdown Spectrometer (CRDS) via introduction through an Automate® carbonate preparation device. Limited additional new carbon isotope data from the Chuar Group (nine data points) were generated using a VG Instruments PRISM II isotope ratio mass spectrometer after sample dissolution in a common acid bath at 90 °C. Isotope compositions reported in the typical delta (δ) notation in permil (‰) versus the VPDB standard. Isotope values were determined by comparison with international [IAEA NBS-18 ($\delta^{13}\text{C} = -5.014\text{‰}$, $\delta^{18}\text{O} = -23.2\text{‰}$), Carrara Marble ($\delta^{13}\text{C} = +2.46\text{‰}$, $\delta^{18}\text{O} = -2.37\text{‰}$), NIST SRM 915B ($\delta^{13}\text{C} = -8.53$)] and laboratory [CRCP90 ($\delta^{13}\text{C} = -4.13\text{‰}$), CRC200 ($\delta^{13}\text{C} = +2.12\text{‰}$), WD-1A ($\delta^{13}\text{C} = -42.61\text{‰}$)] standards. New carbon isotope data reproducibility was better than $\pm 1.0\text{‰}$ (2 s.d.).

Statistical parameter estimation of the mean, variance, minimum, maximum and range of carbon isotope data was accomplished via bootstrapping (Efron, 1979) across select time periods (Supplementary Table 5). Biases in estimating extrema were simulated empirically from repeated resampling, and then applied to adjust distributions for parameter estimation of maximum and minimum values (Efron, 1982). Confidence intervals (95%) for each numerical summary across the selected time periods were generated via the bootstrap empirical distributions, as were pairwise statistical hypothesis tests between each pairwise combination of selected time periods.

The factors that control potential ranges in carbon isotope compositions were evaluated using a previously described transient reaction transport model (Meister et al., 2013; Meister et al., 2019). This model was developed in part to constrain transport and biogeochemical impacts on isotope compositions of the dominant carbon-containing porewater phases. Marine sulfate concentrations, organic carbon content at the sediment–water interface, external methane delivery, isotope fractionation during methanogenesis and marine DIC contents were varied to explore impacts on porewater DIC isotope compositions. Here, complete ranges in porewater $\delta^{13}\text{C}_{\text{DIC}}$ values (including maxima and minima) are explored without predicting specific depths of carbonate authigenesis (in contrast to Laakso and Schrag (2020)). The modelled porewater isotope compositions are thus reflective of all of the possible concretion isotope compositions, resolving potential uncertainties in mineralization depth (e.g., Meister et al., 2019). Model inputs and parameterizations are provided in the Supplementary Materials (“Modeling Approach”), as is a diagram demonstrating how maximum and minimum values were determined (Supplementary Figure 1). Model results are compared to the ancient concretion carbon isotope record to identify potential drivers of temporal variability, they are not intended to recreate specific intervals of the record.

3. Results

Carbonate concretions have been identified in 379 geologic formations. Of these units, carbon isotope data have been compiled or generated from 173, representing ~46% $\delta^{13}\text{C}_{\text{con}}$ coverage. The age distribution of carbonate concretions is not uniform; the vast majority have been identified in units younger than 600 Ma (Fig. 1). An exception to this broad temporal trend is a relatively short-lived, concretion-abundant interval between ~2150 to 1750 Ma (Fig. 2b). Within the Phanerozoic, concretion occurrence generally increases (aside from a few exceptions) up to the modern (Fig. 1c). As has been recognized in a previous compilation (Mozley and Burns, 1993) concretions mostly occur within shale hosts (Fig. 2a) and calcite represents the dominant mineralogy (Fig. 2b).

Carbon isotope compositions range from -54.0 to $+32.5\text{‰}$ for the entire data set. Absolute $\delta^{13}\text{C}_{\text{con}}$ values provide only limited insight into

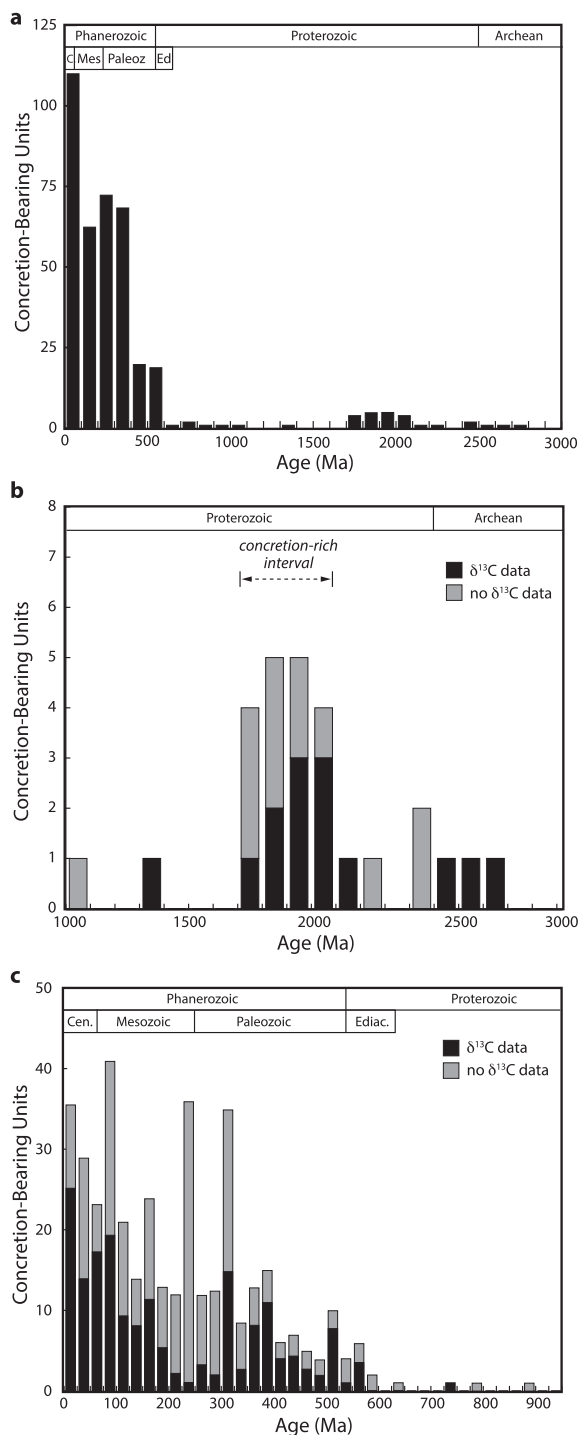


Fig. 1. Abundance of concretion-bearing units through time. (a) Entire distribution in 100-Myr age bins. (b) 3000 to 1000 Ma, notice concretion-rich interval following the Archean Proterozoic boundary. (c) 950 Ma to present in 25-Myr age bins. Panels b and c indicate $\delta^{13}\text{C}$ coverage.

concretion formation mechanisms. These data must be corrected to account for the contemporaneous seawater $\delta^{13}\text{C}$ value, which represents the starting condition that is subsequently modified by shallow diagenetic processes. This correction is relatively unimportant for Cenozoic concretions because seawater $\delta^{13}\text{C}$ does not significantly deviate from 0‰. However, a growing body of primary carbonate (i.e., non-diagenetic) carbon isotope data suggests that seawater $\delta^{13}\text{C}$ was significantly different in earlier time periods (in particular during intervals within the Proterozoic), in some cases reaching values as high as +11 (e.

g., Maheshwari et al., 2010) to as low as -12‰ (e.g., Halverson et al., 2005). In order to account for changes in seawater carbon isotope compositions, the quantity $\Delta^{13}\text{C}_{\text{con-sw}}$ is defined as $\Delta^{13}\text{C}_{\text{con-sw}} = \delta^{13}\text{C}_{\text{con}} - \delta^{13}\text{C}_{\text{sw}}$, where $\delta^{13}\text{C}_{\text{sw}}$ is the contemporaneous seawater carbon isotope composition as determined by either (1) the primarily Phanerozoic curve of Veizer et al. (1999) or (2) stratigraphically nearby non-diagenetic carbonate beds. The $\Delta^{13}\text{C}_{\text{con-sw}}$ parameter presented in Fig. 4 thus reflects specific diagenetic pathways more directly than $\delta^{13}\text{C}_{\text{con}}$. Uncertainties related to the primary carbonate $\delta^{13}\text{C}$ value and temporal variability in isotope fractionation associated with organic matter production (e.g., isotopic differences between contemporaneous marine DIC and organic carbon varying between ~ 30 and 25‰ , Kump and Arthur, 1999) are accounted for by the gray solid and dashed bands in Fig. 3.

Values of $\Delta^{13}\text{C}_{\text{con-sw}}$ exhibit significant changes since ~ 2800 Ma (Fig. 3), as outlined below.

- Archean concretion samples from ~ 2800 , 2603 and 2600 Ma units yield $\Delta^{13}\text{C}_{\text{con-sw}}$ values that range from $+9.9$ to $+15.0\text{‰}$, -4.5 to $+1.8\text{‰}$ and $+0.9$ to $+2.4\text{‰}$, respectively.
- Early Proterozoic concretions (of the ~ 2150 to 1750 Ma interval discussed above) show $\Delta^{13}\text{C}_{\text{con-sw}}$ values that range from -24.5 to $+1.4\text{‰}$. ~ 1400 Ma concretions express $\Delta^{13}\text{C}_{\text{con-sw}}$ from -1.1 to $+1.9\text{‰}$.
- Concretions from a single middle Neoproterozoic site (~ 745 Ma) exhibit $\Delta^{13}\text{C}_{\text{con-sw}}$ values ranging from -15.6 to -7.9‰ .
- Late Neoproterozoic (~ 560 and 555 Ma) carbonate concretions exhibit $\Delta^{13}\text{C}_{\text{con-sw}}$ values from -3.5 to $+5.4\text{‰}$.
- Cambrian to Devonian (542 – 360 Ma) concretions display an increased range in $\Delta^{13}\text{C}_{\text{con-sw}}$, with values extending from ~ -25.3 to $+24.5\text{‰}$.
- Younger concretions within Carboniferous to Permian sedimentary rocks express $\Delta^{13}\text{C}_{\text{con-sw}}$ values extending from -54.6 to $+9.5\text{‰}$.
- Triassic to Holocene concretions yield $\Delta^{13}\text{C}_{\text{con-sw}}$ values ranging from -55.7 to $+31.5\text{‰}$.

For comparison, marine sedimentary authigenic carbonate data (compiled in Supplementary Table 4, after Loyd and Smirnov (2022)) are also provided. Note that sedimentary authigenic carbonates characterized as “modern”, may rather have formed at any time since the ages of the host sediment (host sediment ages provided in Supplementary Table 4). Similarly, carbonate concretions must have formed after deposition of the host rock. However, given that these precipitates form relatively soon after deposition, concretion ages are here approximated as the same as their host sediment. Concretion carbon isotope means, minima, maxima and ranges are provided for the above age groupings in Fig. 4; histograms are displayed in Supplementary Fig. 2, and statistical similarity analyses are provided in Supplementary Table 5.

As with primary carbonate phases, concretions may be altered by later diagenetic processes that overprint original carbon isotope compositions as often indicated by ^{18}O -depleted compositions (Bojanowski et al., 2014; Gross and Tracey Jr, 1966; Seewald, 2003). To screen for potential late diagenetic impacts on the temporal record, plots limited to samples expressing oxygen isotope compositions $> -10\text{‰}$ and $> -5\text{‰}$ have been generated (Supplementary Fig. 3). These plots express similar trends as the complete record, suggesting that later diagenetic alteration does not strongly influence the broad temporal trends in $\Delta^{13}\text{C}_{\text{con-sw}}$.

4. Discussion

The concretion occurrence and carbon isotope data presented here provide a more detailed picture of a temporal variability hypothesized by previous researchers (Melezhik and Fallick, 1996). The potential controls of this distribution are discussed below. Firstly, the quantities of concretion-bearing units and preserved marine sedimentary formations are compared to determine if variability can be explained simply by

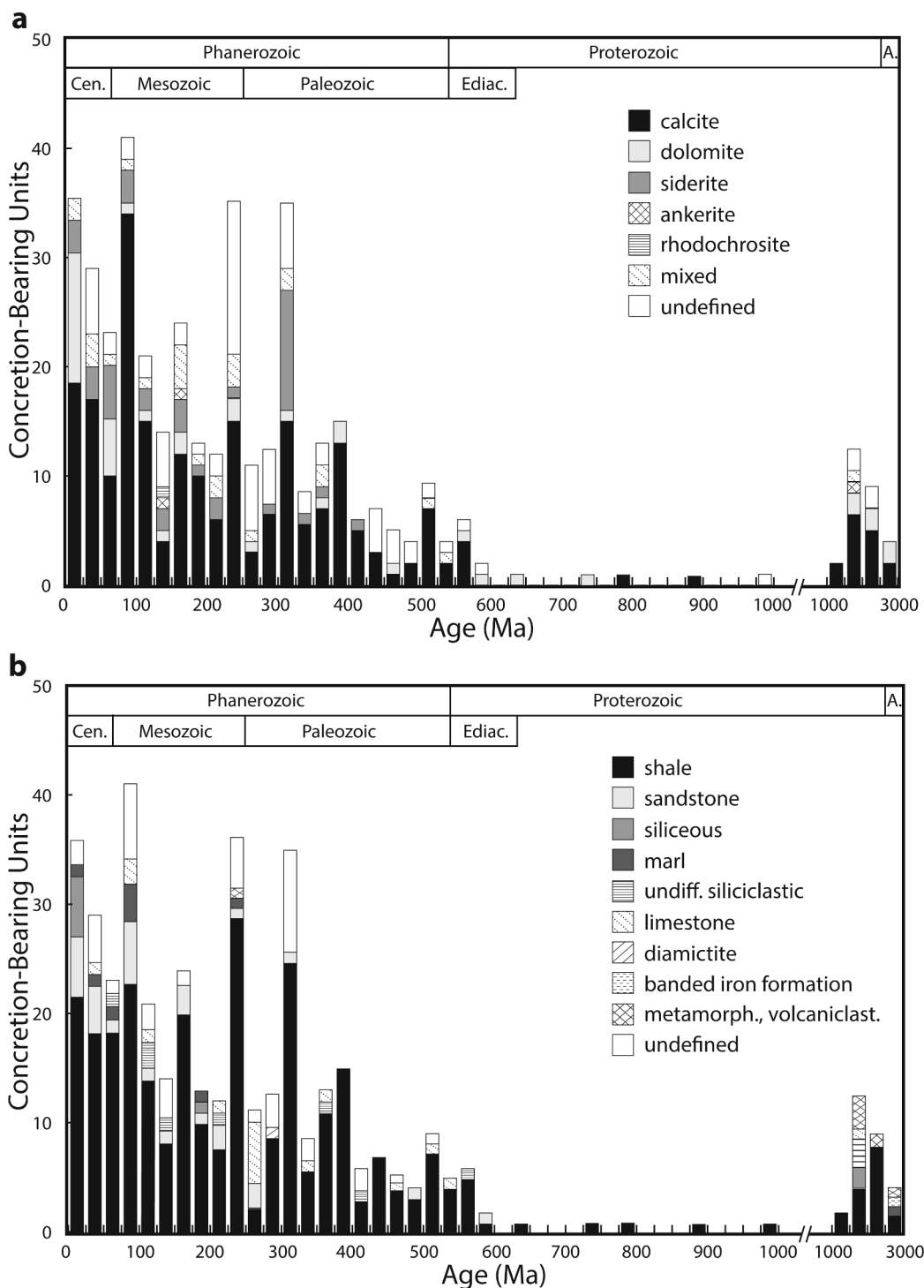


Fig. 2. Concretion (a) mineralogy and (b) host lithology. Note scale compression for 1000 Ma and older bins.

changes in the amount of rock preserved. Then, the major shifts in concretion carbon isotope composition are assessed in the context of potential controls on early marine diagenesis and mineralization.

4.1. Insights from the concretion record

The ability to assess the evolution of Earth-surface environments is increasingly challenging as we move back in time due to the limited preservation of older rocks. In addition, ongoing research shows that the mass of preserved sedimentary rock is not readily explained by erosive processes alone. Instead, changes in the Earth-surface system have likely

impacted the production of sedimentary rock through time (Husson and Peters, 2018; Ronov et al., 1980). Reconstructions of the temporal abundance of passive margins (Bradley, 2008) and the quantity and volume of marine sedimentary rock formations (preserved on the North American continent) correlate with the quantity of concretion-bearing units (Supplementary Fig. 4). Therefore, an environmental signal cannot be confidently identified even though a clear temporal change in concretion-containing units is evident. The concretion abundance record may also be obscured by reporting biases in the literature, the dominant data source for this compilation. As a result, the remaining discussion focuses on concretion carbon isotope data ($\Delta^{13}\text{C}_{\text{con-sw}}$) and

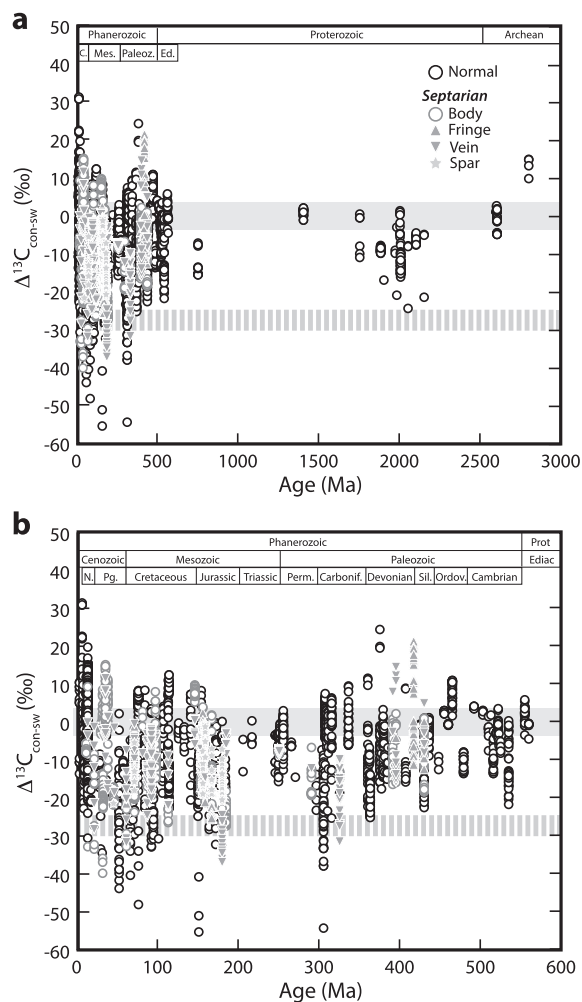


Fig. 3. $\Delta^{13}\text{C}_{\text{con-sw}}$ variability (a) since 3000 Ma and (b) since the latest Proterozoic. Shaded envelope encompasses expected seawater values and dashed line indicates minimum values for organic matter oxidation (-25‰). Normal and septarian concretions and associated crystal habits indicated by symbols.

potential controls on its variability.

The carbon isotope composition of a carbonate concretion is inherited from the porewater DIC from which it precipitates. Since there is only minimal isotope fractionation associated with carbonate mineral production (Emrich et al., 1970; Ohmoto and Rye, 1979), carbonate concretions provide a unique proxy for ancient diagenetic settings. The carbon isotope composition of DIC in porewater reflects a mixture of carbon derived from seawater, the oxidation of organic matter and the oxidation of methane. In addition, methanogenesis exhibits a significant isotope fractionation (Whiticar, 1999) that can further impact porewater DIC. The ranges in isotope composition expressed in marine sediment porewaters result from the relative importance of these different reactions in addition to the transport of carbon-containing reactants and products (Zeebe, 2007). Oxidation- and organic matter-dependent reactions appear to typify much of Earth history, as evidenced by the widespread occurrence of negative values of $\Delta^{13}\text{C}_{\text{con-sw}}$. These reactions require external reactant(s), potentially including aqueous sulfate and particulate iron oxide, and organic matter and/or methane carbon sources. A growing body of research provides insight into the relative temporal abundances of some of these phases. The following discussion explores reactant variability and then connects these trends to specific characteristics of the $\Delta^{13}\text{C}_{\text{con-sw}}$ record to evaluate the evolution of marine diagenetic environments.

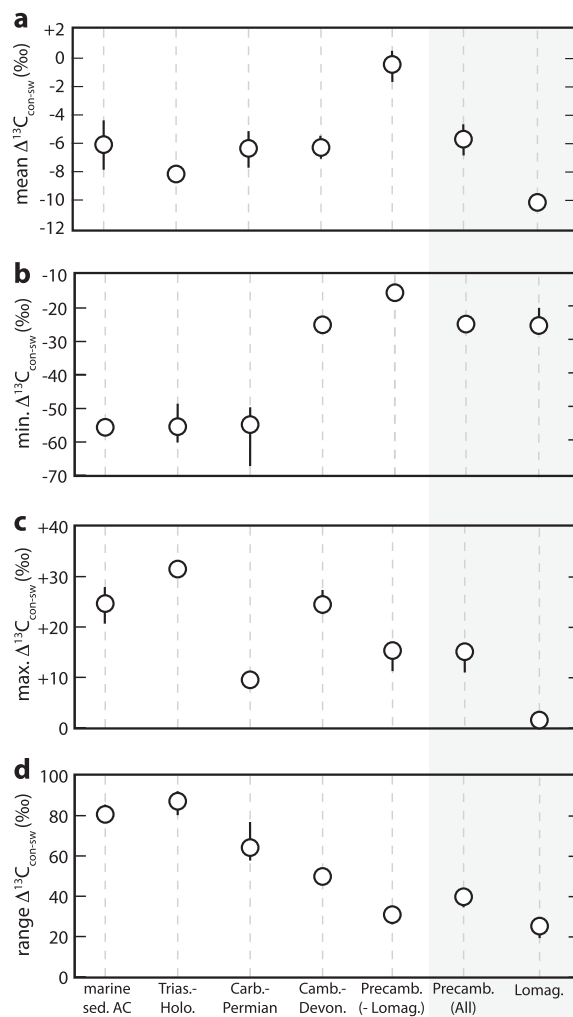


Fig. 4. $\Delta^{13}\text{C}_{\text{con-sw}}$ (a) mean, (b) minimum (min.), (c) maximum (max.) and (d) ranges for different age intervals. Precambrian data provided with (All) and without (- Lomag.) Lomagundi-aged samples. Notice decrease in minimum and increase in maximum and ranges through time.

4.2. Organic matter as a carbon source for carbonate precipitation

The dominant concretion-forming mechanisms in marine sediments involve the anaerobic degradation of organic matter or methane (Claypool and Kaplan, 1974; Coleman, 1993; Irwin et al., 1977). Methane primarily forms by the degradation of organic matter, either directly through fermentation reactions or indirectly through the reduction of carbon dioxide derived from organic matter (Koyama, 1963; McCarty, 1964). Therefore, all of the major reaction pathways that lead to concretion precipitation involve organic matter in one way or another.

The amount of marine carbon buried as organic matter has changed through time (Fig. 5), partially in concert with shifts in the oxidation state of Earth's surface (Krause et al., 2022; Krissansen-Totton et al., 2021; Planavsky et al., 2022). Our ability to assess carbon burial relies primarily on temporal changes in the carbon isotope compositions of primary marine carbonates, which approximately record the isotope composition of oceanic DIC at the time of deposition (Schidlowski et al., 1975). Assuming that marine carbonate $\delta^{13}\text{C}$ changes reflect steady-state oceanic inorganic carbon budgets, increases correspond to enhanced organic carbon burial whereas decreases reflect increased organic carbon destruction (i.e., oxidation) (Kump and Arthur, 1999). Although the $\delta^{13}\text{C}$ composition of limestones and dolostones preserved in the geologic record may not faithfully record original marine

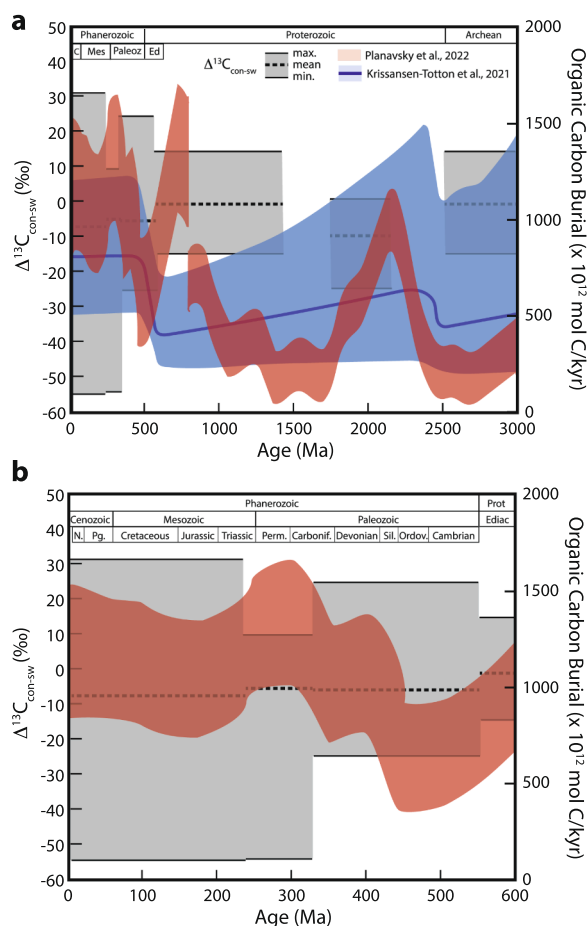


Fig. 5. Marine organic carbon burial and $\Delta^{13}\text{C}_{\text{con-sw}}$ (gray envelopes). (a) Temporal variability since 3000 Ma and (b) 600 Ma. Organic carbon burial data after model reconstructions of Planavsky et al. (2022) and Krissansen-Totton et al. (2021). Organic carbon burial after low erosion rate, low overbank oxidation results of Planavsky et al. (2022) (Fig. 14a from that work), other result show similar trends but with potentially different absolute values.

conditions (e.g., Knauth and Kennedy, 2009), long-lived and global positive carbon isotope excursions are difficult to explain without invoking primary marine drivers. In particular, the ~ 2.3 to 2.1 Ga Lomagundi excursion corresponds to a large $\sim +10\%$ carbonate carbon isotope swing (e.g., Schidlowski et al., 1976) thought to be related to massive deposition of organic matter and an increase in atmospheric O_2 (e.g., Eguchi et al., 2020; Karhu and Holland, 1996). Although the Lomagundi positive isotope excursion has been interpreted as a diagenetic signal related to methane production (Hayes and Waldbauer, 2006), contemporaneous trends in sulfur and sulfur isotope geochemistry are more parsimoniously interpreted as consistent with a primary origin (Planavsky et al., 2012). The Lomagundi event overlaps with the beginning of the concretion-abundant interval between ~ 2.15 to 1.75 Ga (Fig. 1a, b) (Melezhik and Fallick, 1996). In addition to enhanced organic matter burial, contemporaneous changes in the redox state of the oceans at this time may have yielded complementary conditions required to stimulate sedimentary diagenesis, such as the introduction of other oxidants to Earth's surface environment (see section 4.3 below).

Similar, long-lived primary carbonate positive $\delta^{13}\text{C}$ values ($\geq +5\%$) occur between glacial intervals in the post- ~ 800 Ma Cryogenian Period (Halverson et al., 2005). These ^{13}C -enriched values are likewise interpreted to represent the enhanced burial of organic matter (Derry et al., 1992; Des Marais et al., 1992) and recent modeling results support these findings (Kipp et al., 2021; Krause et al., 2022; Krissansen-Totton et al., 2021; Planavsky et al., 2022). Beginning about the same time (~ 750

Ma) and extending toward the Proterozoic–Cambrian boundary, a transition in clay mineral production may have facilitated enhanced burial of organic matter (Kennedy et al., 2006; Kennedy et al., 2002). However, the direct impacts of this transition on atmospheric oxygen contents have been challenged (Tosca et al., 2010). In addition, labile organic matter that is buried in clay-rich sediments can be protected from degradation (Keil et al., 1994), complicating the ability to predict potential impacts of secular changes in clay production on shallow diagenetic environments.

Temporal variability in the total organic carbon (TOC) contents of marine shales also provides support for fluctuating organic carbon burial (Och and Shields-Zhou, 2012; Sperling and Stockey, 2018). Importantly, TOC contents increase significantly across the Neoproterozoic–Cambrian boundary and remain relatively high throughout the Phanerozoic (Sperling and Stockey, 2018) as also supported by modeled reconstructions of organic matter burial rates (Krause et al., 2022; Krissansen-Totton et al., 2021; Planavsky et al., 2022). Shallow-marine diagenesis may have been stimulated as a result of this high organic carbon burial rate.

Recent work has also revealed a profound shift in the nature of marine organic matter between the Cryogenian “Snowball Earth” glacial intervals (~ 659 to 645 Ma). Biomarker data suggest a transition from a dominantly bacterial to a bacterial and eukaryotic marine planktonic biosphere (Supplementary Fig. 5) (Brocks et al., 2017). This expansion in marine biosphere diversity may have heralded contemporaneous changes in organic matter reactivity. Organic matter reactivity impacts the efficiency of remineralization (e.g., Burdige, 2007) and can influence degradation pathway (Meister et al., 2013). However, the relationship between organic matter source (eukaryotic versus non-eukaryotic) and general reactivity remains poorly understood. Therefore, the addition of significant eukaryotic biomass may or may not have increased the reactivity of organic matter and thus stimulated shallow diagenesis. The record of carbonate concretions since ~ 659 to 645 Ma exhibits its own interesting trends, perhaps related to two subsequent biological transitions, the appearance and proliferation of metazoans and land plants (Supplementary Fig. 5).

Partially decayed carcasses of animals, including bones and calcium carbonate or phosphate shells, sometimes occur within carbonate concretions (El Albani et al., 2001; Gaines et al., 2005; Yoshida et al., 2015). Such materials may have provided triggers for localized remineralization and carbonate precipitation since the latest Neoproterozoic. The large accumulation of organic matter associated with decaying animal carcasses provides a local source for anaerobic degradation processes that can cause focused alkalinity increase and thus facilitate carbonate formation (e.g., Duck, 1995). Inorganic mineral phases (shell calcite, aragonite, or phosphate and bone) can also provide nucleation sites for precipitation due in part to the reduced thermodynamic hurdles related to mineral formation on preexisting crystalline materials (Berner, 1980; Sunagawa, 1994).

The arrival of extensive (plant) terrestrial ecosystems during the Silurian (Supplementary Fig. 5) and their expansion thereafter (Gibling and Davies, 2012; Kenrick and Crane, 1997) likely resulted in a more substantial delivery of exogenous organic matter to the oceans. Such remains occur in marine sediments of the Phanerozoic (Sackett et al., 1974). Raiswell and Berner (1986) have demonstrated a shift toward higher C/S ratios in normal marine shales by the Middle Devonian, consistent with increased delivery of terrestrial organic matter (TOM) thereafter. Remineralization of this TOM could promote carbonate concretion authigenesis. Indeed, modern TOM is thought to provide a significant portion of the total organic carbon budget, particularly in coastal marine sediments (Burdige, 2005; Schlünz and Schneider, 2000). However, TOM may be less reactive than marine organic matter (Aller et al., 1996; Burdige, 2005; Hedges et al., 1997), potentially obscuring the potential impacts of increased delivery. Regardless, such a fundamental shift in carbon sources to marine sediments is likely to have impacted shallow marine diagenetic processes in shelf and slope

depositional settings.

4.3. Oxidant availability and its influence on organic matter remineralization

Diagenetic processes in shallow marine sediments (including concretion formation) are impacted by the abundance of organic carbon (Arndt et al., 2013), the availability and nature of which has likely changed through geologic time (see above). Remineralization reactions may or may not require additional external oxidant and thus the fate of buried organic matter is variably tied to oxidant availability. The temporal variability of select oxidants, including sedimentary iron oxide and marine sulfate contents (recognized as important in organic matter remineralization and carbonate authigenesis) is discussed in this section.

The idea that Earth's surface has experienced progressive oxygenation is widely accepted. The structure of this oxygenation however, remains a topic of considerable debate. In addition, progressive oxygenation likely impacted the abundances of specific oxidants through time differently. These oxidant budgets in turn likely imparted a first-order control on sedimentary diagenesis of marine environments by stimulating oxidative degradation of organic matter and methane. The temporal evolutions of oxygen and oxidant availability are outlined below.

4.3.1. Oxygen (O_2)

Atmospheric oxygen concentrations likely provide a first-order control on the oxidation state and oxidant capacity of surface environments (both terrestrial and marine). The oxygen content of the atmosphere is thought to have increased as a result of two major oxygenation events. The first of these corresponds to the ~2.5–2.3 Ga Great Oxidation Event (GOE) and is at least casually linked to photosynthetic O_2 buildup (Holland, 2002). This earlier oxygen increase, however, was probably not permanent, terminating with a return to lower oxygen conditions (Bekker and Holland, 2012; Partin et al., 2013). The second increase in oxygen content is thought to have occurred during the Late Neoproterozoic to early Cambrian (Chen et al., 2015; Sahoo et al., 2012; Scott et al., 2008), may have resulted in the ventilation of portions of the deep ocean and heralded the oxygen-rich conditions exhibited today (Lyons et al., 2014). Phanerozoic atmospheric oxygen contents have also fluctuated, albeit at a higher level (between ~10–100% present atmospheric level) (e.g., Berner and Canfield, 1989; Lenton et al., 2018).

Despite increasing oxygen concentrations in Earth's atmosphere, the oxidation state of the oceans has exhibited its own complexity, driven in part by the evolving atmospheric boundary condition (Canfield, 1998; Lyons et al., 2009). Prior to the GOE Earth's oceans were predominantly ferruginous (iron(II)-rich) at all depths. After the GOE and until the Proterozoic-Phanerozoic boundary, the redox structure shifted to include oxic and/or sulfidic shallow/mid-depth waters over a persistently ferruginous deep ocean, reflecting in part the delivery of sulfate by oxidative weathering on land and its subsequent reduction to hydrogen sulfide in the water column (Lyons et al., 2009; Planavsky et al., 2011; Poulton et al., 2010). In contrast, generally oxygenated oceans typify the Phanerozoic, with low oxygen and sulfidic marine environments restricted to near-shore, productive and/or restricted settings (Anderson and Devol, 1973; Jacobs et al., 1985; Price and Calvert, 1973; Skei, 1983). These marine transitions are relatively coarse; the fine-scale structure of the redox state of the oceans is potentially much more complex and remains the topic of considerable debate (Lyons et al., 2014). Although the *general* transitions in atmospheric and ocean oxidation state are widely accepted, bottom water concentrations of oxidized phases other than oxygen (including iron oxides and dissolved sulfate) are less well constrained. Oxidant availability at the sediment–water interface impacts the degradation potential of sedimentary organic matter and methane and thus provides a first order control on shallow marine diagenesis.

4.3.2. Particulate Iron Oxide

Iron oxide minerals provide an attractive electron acceptor for organic matter and methane oxidation and subsequent concretion precipitation. Iron reduction metabolisms are thought to be relatively ancient, as indicated by iron isotope compositions in rocks as old as ~3.8 Ga (Supplementary Fig. 5) (Craddock and Dauphas, 2011). A compilation of speciation data for shale-hosted iron provides insight into the relative availability of iron oxide through time (Fig. 6). The highly reactive iron fraction (FeHR) includes oxide phases (e.g., hematite, magnetite) and reduced phases (e.g., pyrite and iron carbonate minerals) (Raiswell and Canfield, 1998) and thus can be used to assess the original iron oxide content (before and after reduction) of marine sediments (see below).

Despite changes in the oxidation state of Earth's surface, broadly expressed as an increase in atmospheric and oceanic oxygen through time, the availability of FeHR in marine shale appears relatively static (Fig. 6). Indeed, Sperling et al. (2015) find similarly unchanged iron speciation from the Proterozoic to the early Paleozoic. Iron data have also been screened to exclude samples with FeHR/FeT values greater than 0.38 (the threshold for sediments deposited under anoxic conditions; (Poulton and Raiswell, 2002), to remove samples with elevated FeHR that are unrelated to sedimentary Fe^{3+} delivery. This restricted data set likewise does not show significant variability among the time intervals of interest here. However, iron speciation data are not equally available for the different time periods (Sperling et al., 2015). More continuous population of this data set may reveal temporal variability

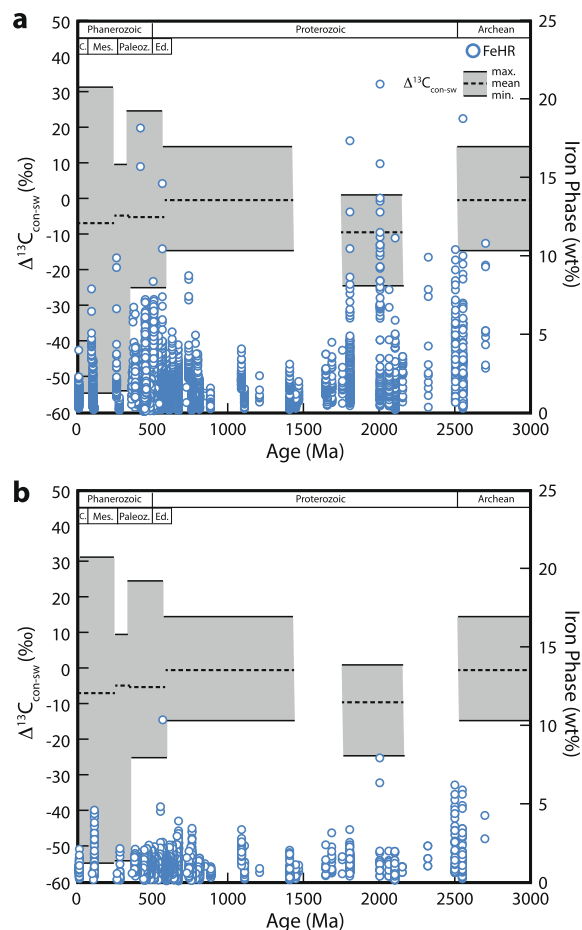


Fig. 6. Iron speciation data and $\Delta^{13}C_{con-sw}$ (gray envelopes). (a) all iron data, (b) data from samples with FeHR/FeT \leq 0.38 wt%. Notice lack of increase in iron contents through time and in particular across the Proterozoic-Paleozoic transition. Correlation plots and iron data references provided in Supplementary Material.

that is missed by this compilation.

4.3.3. Aqueous Sulfate

The understanding of the temporal evolution of marine sulfate concentrations has developed significantly over the past twenty years. This understanding stems from fluid inclusion data (Horita et al., 2002; Lowenstein et al., 2003), sulfur isotope variability (Algeo et al., 2015; Gill et al., 2011; Kah et al., 2004; LaFlamme et al., 2021; Planavsky et al., 2012) and fractionation magnitude experiments (Habicht et al., 2002), modeling (Bernier, 2004; Fakhraee et al., 2018; Fakhraee et al., 2019; Krause et al., 2022; Shi et al., 2022) and the occurrence of marine evaporite deposits in the geologic record (Evans, 2006; Halevy et al., 2012; Wortmann and Chernyavsky, 2007). Sulfate concentrations (Fig. 7) exhibit a transient rise in association with the ~2.3 to 2.1 Ga Lomagundi interval (Planavsky et al., 2012; Salop, 1982; Schröder et al., 2008) which overlaps with the beginning of the relatively concretion-abundant interval at ~2.15 to 1.75 Ga (Melezhik and Fallick, 1996). Evaporite paragenetic data that show halite saturation prior to gypsum/anhydrite may indicate a return to low sulfate concentrations by ~1.9 Ga (Blättler et al., 2018; Pope and Grotzinger, 2003).

At ~1.7 Ga sulfate concentrations have been estimated at ~1.5 mM and remain below ~5 mM until ~750 Ma where sulfate concentrations increase to ~10 ± 5 mM (Blättler et al., 2020; Kah et al., 2004; Krause et al., 2022), similar to the Phanerozoic minimum (Horita et al., 2002; Lowenstein et al., 2003). Within the Phanerozoic, sulfate concentrations

vary (Fig. 7b), reaching up to ~28 mM in the modern (Horita et al., 2002; Lowenstein et al., 2003). This variability is broadly characterized by two stepwise increases, one occurring across the Ediacaran–Cambrian boundary where concentrations are thought to have reached up to ~10 mM in the early Cambrian and the other beginning in the late Paleozoic. The timing of late Paleozoic sulfate increase varies depending on literature source; however most reconstructions display an increase at the beginning or within the Carboniferous. Note that the sulfate records presented in Fig. 7 may not include brief episodes of sulfate fluctuation such as those associated with the Permian–Triassic interval (Luo et al., 2010; Song et al., 2014) and Cretaceous Ocean Anoxic Events (Adams et al., 2010; Ohkouchi et al., 1999).

4.4. Evolving carbon isotope distribution in shallow diagenetic environments throughout Earth history

As discussed above, $\Delta^{13}\text{C}_{\text{con-sw}}$ provides insights into temporal changes in shallow marine diagenesis, particularly when isotope compositions exceed or fall below threshold values. Data mean, maximum, minimum and range values for different age intervals demonstrate significant temporal variability (Fig. 4), perhaps related to evolving marine diagenetic environments. It is important to note that the data-limited Neoproterozoic and older record may be more susceptible to biases associated with local rather than global environmental controls (depositional environment, etc.) compared to the data-replete younger record. We acknowledge that additional data collection may help resolve this potential bias and interpret the concretion carbon isotope variability demonstrated here in the context of broad temporal changes in Earth's surface environment. A lack of clear changes in reactive/oxide iron phases (Fig. 6, Supplementary Fig. 6) suggests that particulate iron oxides do not drive $\Delta^{13}\text{C}_{\text{con-sw}}$ variability. Thus, concretion isotope evolution is discussed in the context of other potential controls in the following discussion.

Prior to ~2.15 Ga, concretions yield values that overlap with or exceed contemporaneous seawater values (i.e., $\Delta^{13}\text{C}_{\text{con-sw}} \geq 0\text{‰}$, Fig. 3). The earliest concretions (~2.8 Ga) express positive $\Delta^{13}\text{C}_{\text{con-sw}}$ values indicating formation as a result of methanogenesis (Dix et al., 1995). Molecular clock studies suggest early evolution of methanogenesis metabolisms, perhaps originating at ~3.8 to 4.1 Ga (Supplementary Fig. 5) (Battistuzzi et al., 2004), well before the formation of these earliest known concretions. Later Archean concretions within ~2.6 Ga rocks express $\delta^{13}\text{C}$ values that do not differ significantly from seawater values (Fig. 3a), suggesting a dominantly marine DIC or primary carbonate mineral dissolution source.

The prevalence of near neutral $\Delta^{13}\text{C}_{\text{con-sw}}$ values during the Precambrian (Fig. 3) may reflect the combined effects of low sulfate availability and high marine DIC contents. As confirmed by model results, lower sulfate concentrations limit porewater oxidation of sedimentary organic matter and methane and preclude severe decreases in $\delta^{13}\text{C}_{\text{DIC}}$ (Fig. 8 and Supplementary Fig. 7) and thus $\Delta^{13}\text{C}_{\text{con-sw}}$. This is consistent with previous modelling work exploring impacts of low sulfate concentration on porewater and authigenic carbonate $\delta^{13}\text{C}$ (Laakso and Schrag, 2020). Marine DIC contents may have been relatively high early in Earth history as supported by muted variability in marine $\delta^{13}\text{C}$ (Bartley and Kah, 2004) and carbonate fabrics that indicate rapid precipitation (Grotzinger and James, 2000). Under elevated marine DIC conditions, shallow porewaters would be buffered against isotope modification by diagenesis. The potential impacts of an increased marine DIC reservoir are demonstrated in Fig. 9. Importantly, under low sulfate and high marine DIC conditions, porewater $\delta^{13}\text{C}_{\text{DIC}}$ variability is diminished, manifested primarily as an increase in minimum values. Under higher sulfate concentrations, the impacts of increasing marine DIC are less substantial. Therefore, high marine DIC values during the Precambrian may have contributed to the limited variability observed in $\Delta^{13}\text{C}_{\text{con-sw}}$.

Conclusively oxidation-derived carbonate concretions first appear at

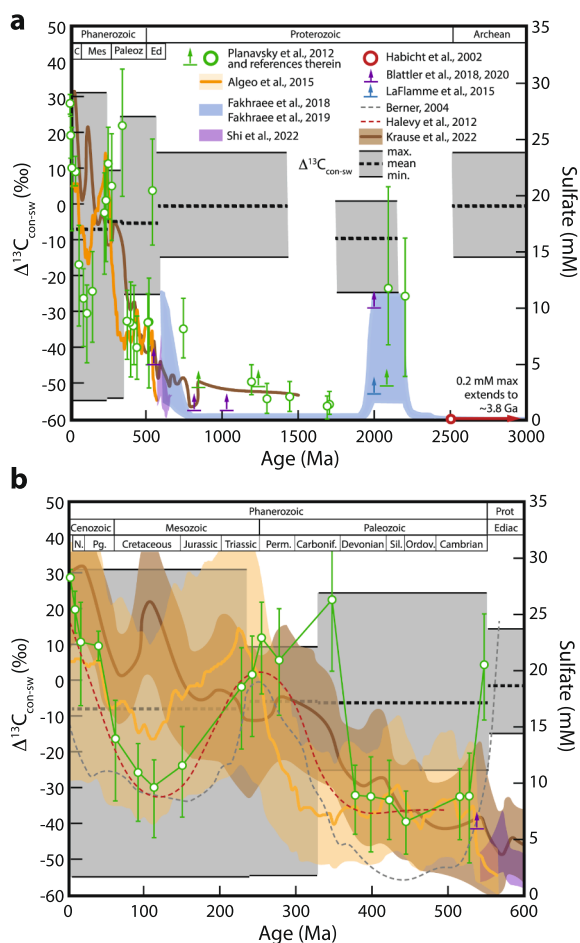


Fig. 7. Marine sulfate concentrations and $\Delta^{13}\text{C}_{\text{con-sw}}$ (gray envelopes). (a) Temporal variability since 3000 Ma and (b) 600 Ma. Sulfate concentrations from Planavsky et al. (2012), MSR-method of Algeo et al. (2015), Fakhraee et al. (2018), Fakhraee et al. (2019), Shi et al. (2022), Habicht et al. (2002), Bernier (2004), Halevy et al. (2012), Blättler et al. (2018), Blättler et al. (2020), LaFlamme et al. (2021) and Krause et al. (2022).

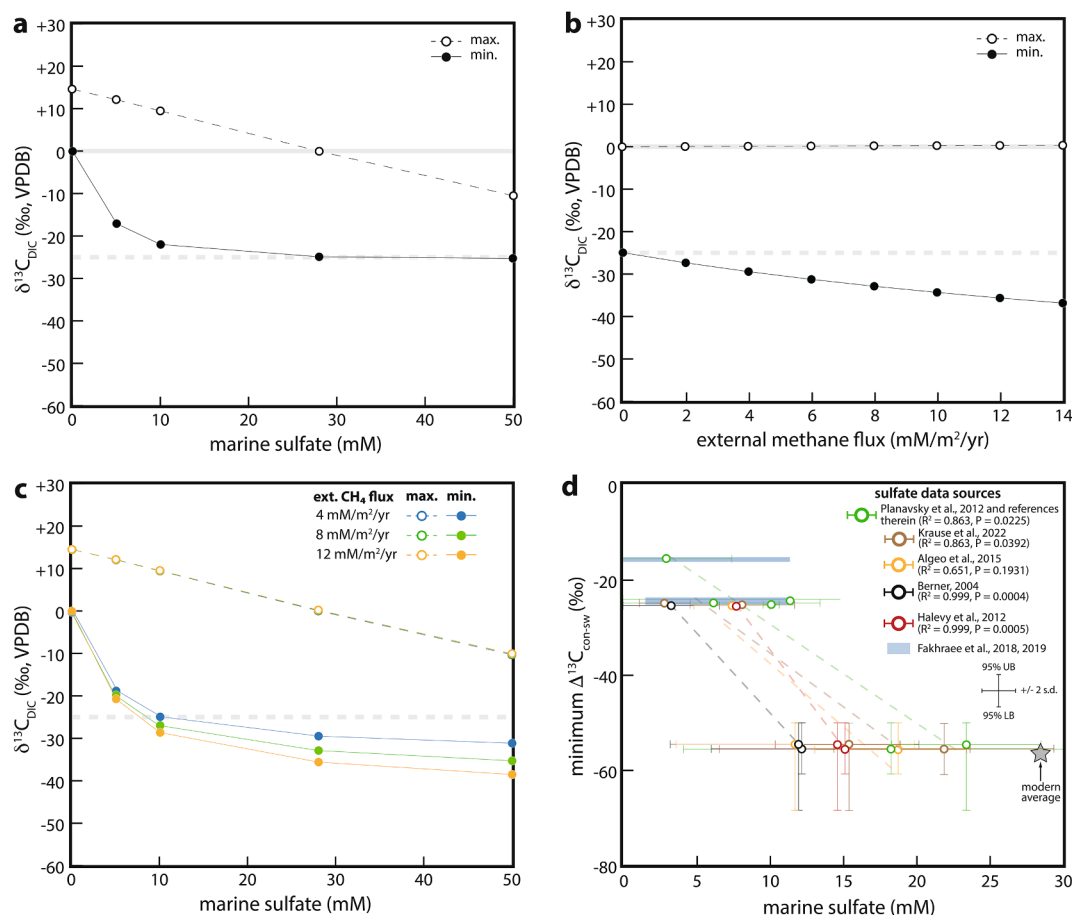


Fig. 8. Porewater model results demonstrating potential controls on $\delta^{13}\text{C}_{\text{DIC}}$ and comparison to concretion record. Solid and dashed gray lines in a–c represent marine DIC and organic matter $\delta^{13}\text{C}$, respectively. (a) impact of marine sulfate content. Note that as sulfate concentrations increase, both $\delta^{13}\text{C}_{\text{DIC}}$ minimum and maximum values decrease. (b) impact of external methane flux under modern marine sulfate concentrations. External methane $\delta^{13}\text{C}$ values are assigned the value achieved at the base of the modeled domain, deviations from this value impact the minimum $\delta^{13}\text{C}_{\text{DIC}}$. Note that as external methane input increases, $\delta^{13}\text{C}_{\text{DIC}}$ minimum values decrease and yield compositions below the organic matter $\delta^{13}\text{C}$ value. (c) impact of marine sulfate content under variable external methane flux (ext. CH_4 flux). Increased sulfate contents yield decreased $\delta^{13}\text{C}_{\text{DIC}}$ minimum and maximum values similar to overall trends observed in a. Note that $\delta^{13}\text{C}_{\text{DIC}}$ depletions produce minimum values that drop well below the organic matter $\delta^{13}\text{C}$ value under high sulfate conditions. Maximum data trends overlap. In a–c, $\alpha_{\text{methane-DIC}} = 0.94$ and the isotopic difference between methane and DIC was maintained at $\sim 75\%$. (d) comparison between marine sulfate concentrations and minimum $\Delta^{13}\text{C}_{\text{con-sw}}$ for the age groupings discussed in the text. Blue bands represent ranges from Fakraee et al., 2018, 2019, all other data are sulfate concentration averages. Notice decrease in minimum isotope compositions with increasing sulfate content, similar to minimum model data in c. Linear regressions and correlation strengths also provided.

~ 2.15 Ga. In fact, all concretion-hosting units between ~ 2.15 and 1.75 Ga include samples with predominantly negative $\Delta^{13}\text{C}_{\text{con-sw}}$ (Fig. 3a). The $\Delta^{13}\text{C}_{\text{con-sw}}$ values extend down to $\sim -25\%$, consistent with at least partial carbon incorporation from organic matter, methane or both (Melezhik and Fallick, 1996). The $\Delta^{13}\text{C}_{\text{con-sw}}$ value of Lomagundi concretions (and other Precambrian-aged concretions) is constrained by nearby limestones considered to reflect primary marine DIC (see Results). In this regard, the ^{13}C -depleted $\Delta^{13}\text{C}_{\text{con-sw}}$ values of the Lomagundi interval should not be impacted by potential facies dependency of primary $\delta^{13}\text{C}$ values (Prave et al., 2022). In addition, the limestone $\delta^{13}\text{C}$ values used to constrain $\Delta^{13}\text{C}_{\text{con-sw}}$ do not exceed $+5.4\%$ (Supplementary Table 1) and thus do not drive the low $\Delta^{13}\text{C}_{\text{con-sw}}$ during this interval.

Intriguingly, the Lomagundi interval post-dates the GOE and coincides with a transient increase in marine sulfate concentration (Planavsky et al., 2012). Concretions of the Lomagundi interval express $\Delta^{13}\text{C}_{\text{con-sw}}$ values significantly lower than the preceding and following Precambrian (Fig. 4), perhaps testament to a significant control of increased marine sulfate on porewater DIC (see Fig. 8a). Concretions with the lowest $\Delta^{13}\text{C}_{\text{con-sw}}$ values formed during the highest marine sulfate concentrations (up to ~ 11 mM, Fakraee et al., 2019; Planavsky et al., 2012) of the Lomagundi interval (Fig. 7a). Thereafter, values

increase but remain negative until ~ 1.75 Ga, despite an apparent massive drawdown in marine sulfate at the tail end of the Lomagundi event (Planavsky et al., 2012). Unfortunately, marine sulfate concentrations are not well resolved between the sulfate “crash” and ~ 1.75 Ga. Constraining sulfate concentrations in this interval would provide additional insight.

The next occurrence of carbonate concretions is reported in the ~ 1.4 Ga Xiamaling Formation. These concretions express $\Delta^{13}\text{C}_{\text{con-sw}}$ near 0% , interpreted to represent a marine DIC carbon source (Liu et al., 2019) rather than one that requires oxidative processes. Sulfate concentrations were relatively low at 1.4 Ga (Fig. 7), perhaps explaining the return to near neutral $\Delta^{13}\text{C}_{\text{con-sw}}$. The next youngest reported concretions occur in shales of the ~ 745 Ma Kwagunt Formation of the Chuar Group (Dehler et al., 2005). These concretions exhibit $\Delta^{13}\text{C}_{\text{con-sw}}$ values ranging from ~ -15 to $\sim -7\%$ (supplemented with new data reported here) and a return to at least partial carbon derivation from the oxidation of organic matter and/or methane. Intriguingly, sulfate concentrations may have been relatively high during this time interval (Kah et al., 2004), which was followed by subsequent decreases associated with Neoproterozoic glacial intervals (Hurtgen et al., 2002). Thus prior to the Cambrian, low $\Delta^{13}\text{C}_{\text{con-sw}}$ values coincide with intervals of transient high marine sulfate concentrations.

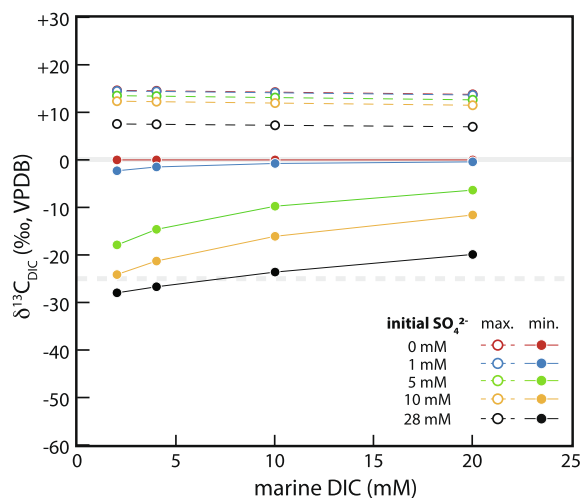


Fig. 9. Modeled variability in $\delta^{13}\text{C}_{\text{DIC}}$ as a function of marine DIC content across a range of marine sulfate concentrations. Increasing marine DIC yields higher $\delta^{13}\text{C}_{\text{DIC}}$ minima except under the 0 mM sulfate condition. This increase is more pronounced at lower marine sulfate concentrations. The $\delta^{13}\text{C}_{\text{DIC}}$ maxima are relatively invariant.

Negative $\Delta^{13}\text{C}_{\text{con-sw}}$ values dominate the relatively well-resolved Phanerozoic record thereafter (Fig. 3), when marine sulfate concentrations were high. Indeed, mean $\Delta^{13}\text{C}_{\text{con-sw}}$ values are significantly lower in the Phanerozoic compared to non-Lomagundi Precambrian counterparts (Fig. 4a). Phanerozoic mean $\Delta^{13}\text{C}_{\text{con-sw}}$ values range from ~ -7.9 to -5.6% whereas the non-Lomagundi Precambrian mean $\Delta^{13}\text{C}_{\text{con-sw}}$ value is $\sim -0.5\%$ (Fig. 4). This decrease demonstrates the oxidative impact of a growing marine sulfate reservoir. Intriguingly, the mean $\Delta^{13}\text{C}_{\text{con-sw}}$ value remains relatively stable throughout the Phanerozoic, despite a subsequent increase in marine sulfate during the mid- to late Paleozoic. The static Phanerozoic mean $\Delta^{13}\text{C}_{\text{con-sw}}$ values developed, in part, as a result of the expansion of the concretion carbon isotope record to include compositions both depleted and enriched in ^{13}C (Fig. 4). The implications of this expansion as related to changing minimum and maximum $\Delta^{13}\text{C}_{\text{con-sw}}$ are discussed below.

Early Paleozoic concretions (Cambrian to Devonian samples) express a minimum $\Delta^{13}\text{C}_{\text{con-sw}}$ value that extends down to $\sim -25\%$, the approximate concurrent organic matter composition. This minimum value is similar to that of the Lomagundi interval (Fig. 4, Supplementary Table 5). Reported marine sulfate concentrations are comparable for these two time intervals, reaching up to ~ 10 mM (Fig. 7). This similarity underscores the control of marine sulfate concentrations on $\Delta^{13}\text{C}_{\text{con-sw}}$. $\Delta^{13}\text{C}_{\text{con-sw}}$ values do not drop below -25% until ~ 325 Ma (Figs. 3 and 4), following reported elevated marine sulfate concentrations in the Carboniferous (Berner, 2004; Gill et al., 2007; Halevy et al., 2010) and representing the first conclusive evidence for methane oxidation-derived inorganic carbon. Similar low isotope compositions persist throughout the remaining record (see minimum $\Delta^{13}\text{C}_{\text{con-sw}}$ values in Fig. 4). These data imply that the AOM pathway has been an important methane consumption and concretion producing reaction since at least ~ 325 Ma and perhaps earlier (methane oxidation-derived concretions need not produce values below -25% if other carbon sources also contributed). Modern marine sediments often show porewater $\delta^{13}\text{C}_{\text{DIC}}$ minima that approach but do not drop below the organic matter value despite active AOM, suggesting quantitative oxidation of locally produced methane by sulfate in shallower sediments (Meister et al., 2019). Modeling results indicate that both high marine sulfate and an external source of methane are required to produce isotope compositions significantly lower than -25% (Fig. 8 and Supplementary Fig. 7). The degree of ^{13}C depletion below -25% ultimately depends on marine sulfate content, the amount of methane entering the system and its $\delta^{13}\text{C}$.

Perhaps not surprisingly, non-concretionary methane cold-seep authigenic carbonates express similarly diagnostic, low $\delta^{13}\text{C}$ values at about the same time. The transition to conclusively methane-oxidation-derived seep carbonates has likewise been attributed to increased marine sulfate concentrations (Bristow and Grotzinger, 2013). The Paleozoic appearance of diagnostically low concretion and seep-carbonate $\Delta^{13}\text{C}_{\text{con-sw}}$ values did not result from the concurrent evolution of organisms capable of AOM as these lineages are relatively ancient, perhaps existing since ~ 2.6 to 2.8 Ga (Supplementary Fig. 5) (Battistuzzi et al., 2004; Hinrichs, 2002).

The relationship of AOM-derived authigenic carbonate to temporal delivery of external methane is more difficult to resolve. We speculate that the generation of significant methane accumulations may in part be related to enhanced organic carbon burial in the Phanerozoic (from marine and/or terrestrial sources, see above). This methane could then be delivered to shallow sediments relatively quickly (perhaps through methane hydrate dissolution, for example) and oxidized to generate the severe ^{13}C depletions diagnostic of AOM. A negative correlation between mean organic carbon burial rates and minimum $\Delta^{13}\text{C}_{\text{con-sw}}$ values (that also drop below -25% , Fig. 10) supports this assertion. Constraining the temporal distribution of large methane reserves is beyond the scope of this work, but may provide additional insight.

4.5. Identifying dominant controls on carbon isotope minima and maxima of inorganic carbon

4.5.1. $\delta^{13}\text{C}$ minima in the AOM zone

As discussed above, sulfate appears to play an integral role in governing Earth's shallow marine diagenetic environments. The relationship between marine sulfate concentration and concretion isotope compositions is emphasized in Fig. 8d. This plot demonstrates a strong negative correlation between the sulfate content and minimum $\Delta^{13}\text{C}_{\text{con-sw}}$ during the time intervals discussed above. Encouragingly, this correlation mimics the porewater minimum $\delta^{13}\text{C}_{\text{DIC}}$ model results of Fig. 8c where the impacts of changing marine sulfate contents are displayed under variable external methane flux. Ultimately these results demonstrate that marine sulfate concentrations and the delivery of external methane dictate the minimum $\delta^{13}\text{C}_{\text{DIC}}$ (and $\Delta^{13}\text{C}_{\text{con-sw}}$) values generated in the AOM zone.

4.5.2. $\delta^{13}\text{C}$ maxima in the methanogenic zone

Collectively, Phanerozoic concretions express $\Delta^{13}\text{C}_{\text{con-sw}}$ values that are consistent with oxidation and methane-producing reactions. The increase in the range in isotope compositions within the Phanerozoic is

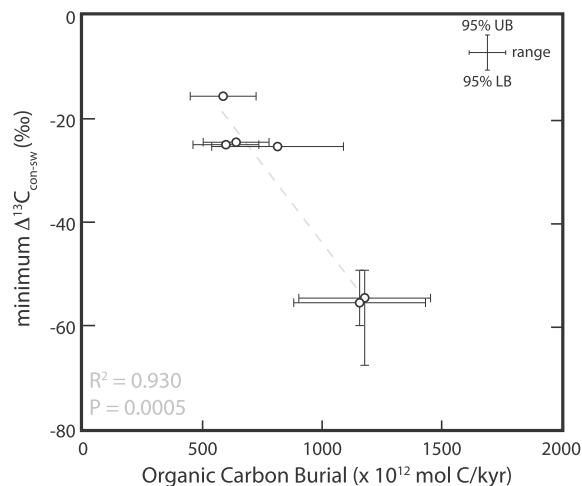


Fig. 10. Comparison between organic carbon burial and minimum $\Delta^{13}\text{C}_{\text{con-sw}}$ for the age groupings discussed in the text.

manifested as both a decrease in minimum and an increase in maximum values (Figs. 3 and 4). As discussed above, sulfate appears to be an important external oxidant as revealed by relationships between sulfate concentration and $\Delta^{13}\text{C}_{\text{con-sw}}$ data. However, the coincident increase in the abundance of conclusively methanogenesis-derived concretions (as indicated by positive $\Delta^{13}\text{C}_{\text{con-sw}}$) is not straightforwardly attributable to increasing sulfate concentrations.

It has been proposed that an increase in the quantity of organic matter delivered to the sediment–water interface may dictate the relative importance of concretion-yielding diagenetic reactions, such that higher amounts promote organic matter persistence to the deeper methanogenesis zone (Mozley and Burns, 1993). In this regard, the increase in the quantity of organic matter in Phanerozoic compared to Neoproterozoic marine sediments recognized by Sperling and Stockey (2018) and supported by model reconstructions (Krause et al., 2022; Krissansen-Totton et al., 2021; Planavsky et al., 2022) may have promoted the expansion of methanogenesis (Sivan et al., 2007). However, maximum $\Delta^{13}\text{C}_{\text{con-sw}}$ values do not show significant correlation with organic carbon burial (Fig. 11a). Fig. 11b and Supplementary Fig. 8

show variability in modeled maximum $\delta^{13}\text{C}_{\text{DIC}}$ values as a function of TOC deposited at the seafloor. Note that the global organic carbon burial rate does not dictate the specific quantity of TOC deposited on the seafloor at any given location. However, broad increases in organic carbon burial are likely to lead to generally higher TOC delivery globally, explaining the motivation behind panel comparisons in Fig. 11. As initial TOC increases so does the maximum $\delta^{13}\text{C}_{\text{DIC}}$; however isotope compositions do not exceed $\sim +15\text{‰}$ (Fig. 11b, Supplementary Fig. 8). Meister et al. (2019) demonstrate this maximum threshold under modern marine sulfate concentrations (28 mM) and new model results show that lower sulfate concentrations do not significantly increase $\delta^{13}\text{C}_{\text{DIC}}$ maximum values. Thus the $\Delta^{13}\text{C}_{\text{con-sw}}$ values above $\sim +20\text{‰}$ commonly expressed in the Phanerozoic record cannot be accounted for by organic carbon burial alone.

It has been demonstrated that increased sedimentation rates lead to faster organic matter burial and degradation in the deeper methanogenesis zone (Burns and Baker, 1987; Pisciotto and Mahoney, 1981; Scotchman, 1991), largely due to limitations associated with sulfate diffusion from the overlying water column. As yet, no data have been reported that indicate an increased sedimentation rate in the Phanerozoic compared to earlier times. Organic matter reactivity can also impact degradation mechanisms. Similar to increased sedimentation rate, less reactive organic matter degrades more slowly and can persist to deeper sediment depths to experience preferential degradation in the methanogenesis zone (Meister et al., 2019). Thus, higher proportions of more refractory organic matter can cause porewater DIC to become more ^{13}C -enriched with depth. The evolution of organic matter reactivity is not well known, but the arrival and diversification of terrestrial plants may have prompted the delivery of less reactive organic material (Aller et al., 1996; Burdige, 2005; Hedges et al., 1997) to marginal environments since the Silurian (Kenrick and Crane, 1997; Raiswell and Berner, 1986). Maximum $\Delta^{13}\text{C}_{\text{con-sw}}$ values, however, show an increase well before the appearance of land plants (Supplementary Fig. 5). Furthermore, significant decreases in organic matter degradation rate are unable to account for porewater DIC ^{13}C enrichments above $\sim +10\text{‰}$ in the methanogenesis zone (Meister et al., 2019) like those expressed in the concretion record. Whereas sedimentation rate and organic matter quantity and reactivity may impact organic matter degradation mechanisms, these factors alone cannot explain the observed data.

Another more speculative explanation involves an increase in the magnitude of carbon isotope fractionation during methanogenesis. Fractionation factors between methane and DIC ($\alpha_{\text{methane-DIC}}$) determined from culture and modern porewater data are between 0.95 and 1.0 (Londry et al., 2008; Whiticr et al., 1986). Some modern marine sediments, however, express $\delta^{13}\text{C}_{\text{DIC}}$ maxima that are difficult to reconcile with low fractionation magnitudes (Meister et al., 2019). In addition, the concretion record suggests that higher maximum porewater $\delta^{13}\text{C}_{\text{DIC}}$ compositions occurred in more recent marine sediments, exceeding the values that can be reached by using the experimentally determined fractionation factors mentioned above. It has been suggested that substrate limitation during AOM promotes reaction reversibility as part of the Wood-Ljungdahl pathway and that this reversibility can lead to isotopic fractionation that approaches theoretical equilibrium magnitudes (Yoshinaga et al., 2014). Similar reversibility may affect isotope fractionation during methanogenesis as suggested by some culture experiments conducted under substrate limited conditions (Botz et al., 1996; see comparison in Meister and Reyes (2019)) and isotope separations between co-occurring porewater DIC and methane recognized in porewaters of many marine sediments (e.g., Galimov and Kvenvolden, 1983; Heuer et al., 2009; Meister et al., 2019; Paull et al., 2000; Pohlman et al., 2008). It is conceivable that under extreme substrate limitation (which is common in sub-seafloor environments) the fractionation factor may approach the theoretical low-temperature equilibrium value ($\alpha_{\text{methane-DIC}} = 0.93$, Bottinga, 1969; Horita, 2001).

To explore the effect of the fractionation factor on maximum $\delta^{13}\text{C}_{\text{DIC}}$, model experiments were conducted at variable $\alpha_{\text{methane-DIC}}$ (from 0.92 to

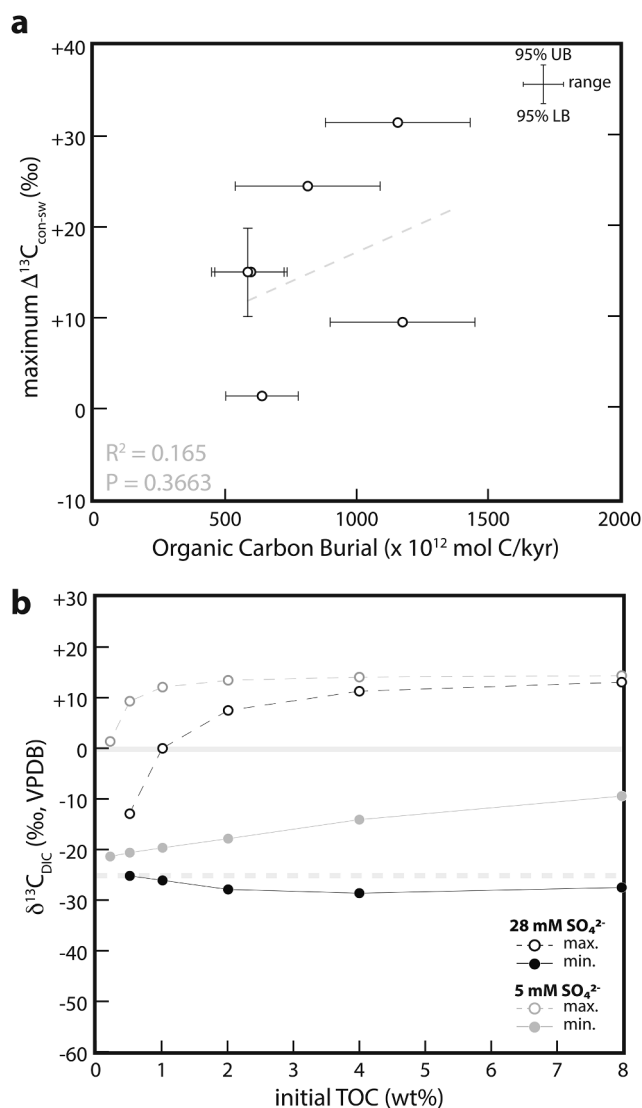


Fig. 11. Impacts of organic carbon burial on isotope compositions. (a) Comparison between organic carbon burial and maximum $\Delta^{13}\text{C}_{\text{con-sw}}$ for the age groupings discussed in the text. (b) Modeled variability in $\delta^{13}\text{C}_{\text{DIC}}$ as a function of total organic carbon (TOC) deposited at the sediment water interface. As TOC contents increase $\delta^{13}\text{C}_{\text{DIC}}$ maximum values increase, but do not exceed $\sim +15\text{‰}$.

0.98, Supplementary Figs. 9 and 10). In these experiments, methane was sourced entirely from within the model domain (i.e., no external methane flux imposed). Maximum $\delta^{13}\text{C}_{\text{DIC}}$ values increased at lower fractionation factors, reaching up to $\sim +9\text{‰}$ (at $\alpha_{\text{methane-DIC}} = 0.92$). However, in this most extreme scenario the isotopic separation between methane and DIC becomes very high ($\sim 100\text{‰}$) and exceeds differences commonly observed in measured profiles. Increasing the external methane flux did not significantly change maximum $\delta^{13}\text{C}_{\text{DIC}}$ when external methane was assigned the $\delta^{13}\text{C}$ composition of the in-situ methane produced at the bottom of the model domain (Supplementary Figs. 9 and 10). Thus, increased isotope fractionation alone cannot account for the highly positive $\Delta^{13}\text{C}_{\text{con-sw}}$ values expressed in the concretion record.

One mechanism that could promote extreme ^{13}C enrichment of porewater DIC involves equilibration with externally derived methane exhibiting a relatively high $\delta^{13}\text{C}$. Such methane can form through thermogenic processes and exhibit isotope compositions near $\sim -40\text{‰}$. Hypothetically, equilibration between thermogenic methane and DIC could result in $\delta^{13}\text{C}_{\text{DIC}}$ values up to $\sim +30$ to $+40\text{‰}$ if the methanogenic reaction is reversible (such that isotope exchange occurs between methane and DIC) and an isotope offset of ~ 70 to 80‰ is maintained. Such a process may in part explain the very high $\delta^{13}\text{C}_{\text{DIC}}$ values recognized at some Cascadia Margin sites (Heuer et al., 2009), although other factors including gas escape to the water column may also play a role (Birgel et al., 2015; Meister et al., 2019). Despite the poorly understood complexities involved in isotope fractionation during methanogenesis and the potential role of equilibration, the mechanisms of ^{13}C enrichments and depletions in porewater DIC may both involve the influx of external methane. As argued above, methane formation (thermogenic or biogenic) may have been stimulated as a result of enhanced organic carbon burial during the Phanerozoic, thus providing a singular driver for the roughly contemporaneous expansion in $\Delta^{13}\text{C}_{\text{con-sw}}$ range.

4.6. Implications for the $\delta^{13}\text{C}$ of authigenic carbonate

Modern authigenic carbonates form within marine sediments as a result of similar reactions to those proposed for carbonate concretions. In fact, carbonate concretions are thought to represent ancient analogs to modern authigenic carbonates (Loyd and Berelson, 2016). This connection has been confounded in part as a result of the inability to identify core-recovered carbonate as concretionary in nature (core sampling limits the ability to characterize the three-dimensional structure of large objects). The similarity between the carbon isotope composition of authigenic carbonate ($\delta^{13}\text{C}_{\text{auth}}$) and Triassic to Holocene $\Delta^{13}\text{C}_{\text{con-sw}}$ values (Fig. 4) provides further support to the proposed analogy. Thus, the concretion-based record presented here may provide insight into the evolution of $\delta^{13}\text{C}_{\text{auth}}$ through time.

As with the carbon isotope composition of carbonate concretions, $\delta^{13}\text{C}_{\text{auth}}$ is likely to have changed as a result of broad changes in the oxidation state of marine bottom waters. Previous work aimed at exploring the impact of authigenic carbonate precipitation on global carbon budgets and marine $\delta^{13}\text{C}_{\text{DIC}}$ hinges intimately on constraining an average $\delta^{13}\text{C}_{\text{auth}}$ value (Schrag et al., 2013). Indeed, Schrag et al. (2013) and Laakso and Schrag (2020) propose that average $\delta^{13}\text{C}_{\text{auth}}$ values may have been different in the past and this inference is supported by the Precambrian $\Delta^{13}\text{C}_{\text{con-sw}}$ record. When data outside the Lomagundi interval are considered, mean Precambrian $\Delta^{13}\text{C}_{\text{con-sw}}$ values differ significantly from other time intervals (Fig. 4). The average Precambrian non-Lomagundi $\Delta^{13}\text{C}_{\text{con-sw}}$ value is very near neutral ($\sim -0.5\text{‰}$) and indistinguishable from contemporaneous primary carbonate. Therefore, according to this concretion data set, burial of Precambrian authigenic carbonate would have had little impact on marine $\delta^{13}\text{C}$ variability. Once marine sulfate concentrations exceeded ~ 5 mM (during brief transient intervals in the Precambrian or otherwise), mean $\Delta^{13}\text{C}_{\text{con-sw}}$ values consistently lie between ~ -10 and $\sim -5\text{‰}$. These compositions agree with recent findings of Laakso and Schrag (2020), are comparable to,

somewhat higher than approximate $\delta^{13}\text{C}_{\text{auth}}$ values proposed by Schrag et al. (2013), and considerably higher than the estimated modern average $\delta^{13}\text{C}_{\text{auth}}$ value of $-20.5 \pm 3.5\text{‰}$, based on compiled pore water geochemical data (Bradbury and Turchyn, 2019). Differences in mean values may in part be explained by the exclusion of non-concretionary, seafloor methane seep carbonates and/or preferential retention of methanogenesis-formed carbonate in the sampled concretion record.

5. Conclusions

Carbonate concretions primarily occur in Phanerozoic rock units and a concretion-rich interval between ~ 2.15 and 1.75 Ga that overlaps with the enigmatic Lomagundi carbon isotope excursion (Melezhik and Fallick, 1996). This distribution may result from preferential formation during these time intervals, but correlation with the abundance of preserved sedimentary rock precludes identification of an environmental signal in the concretion occurrence record. In contrast, the concretion isotope record provides important information about shallow marine diagenetic environments. Negative $\Delta^{13}\text{C}_{\text{con-sw}}$ values dominate the Phanerozoic and Lomagundi interval and correlate with periods exhibiting high marine dissolved sulfate concentrations and organic carbon burial rates. Concretions with conclusively AOM carbon isotope signals appear at ~ 325 Ma and are relatively common in the younger record, likely in response to a Paleozoic rise in marine sulfate concentrations and significant delivery of external methane. The Phanerozoic record also shows an increase in $\Delta^{13}\text{C}_{\text{con-sw}}$ through time perhaps resulting from increased input of thermogenic methane and isotopic equilibration with porewater DIC. Ultimately, the concretion record demonstrates coeval evolution of Earth's primary marine and shallow diagenetic environments, in part related to shifting redox conditions.

Declaration of Competing Interest

The authors declare that they have no known competing financial interests or personal relationships that could have appeared to influence the work reported in this paper.

Acknowledgements

We thank Julie Unson and Miguel Rincon for analytical assistance and Mary Droser for providing Chuar Group samples. Jon Husson provided integral rock abundance data from the Macrostrat database. Insightful communications with Peter Mozley, Doug LaRowe, Kristen Bergmann, Eric Sperling, Maggie Osborn and David Ware and early reviews provided by Ben Gill, Leanne Hancock and one anonymous reviewer were highly beneficial to this manuscript.

Funding: This research was funded in part by CSUF 2016-17 Incentive, CSUF 2018-19 JrSr and CSUF 2019 RSCA grants awarded to S.J.L. BL funded by the BMBF MARE:N project "Anthropogenic impacts on particulate organic carbon cycling in the North Sea (APOC)" (03F0874A).

Appendix A. Supplementary material

Supplementary material related to this manuscript includes tabulated concretion and modern authigenic carbonate data, statistical analysis results, a description of the applied reaction transport model, histograms of $\Delta^{13}\text{C}_{\text{con-sw}}$ data at different time intervals, the temporal trend of $\Delta^{13}\text{C}_{\text{con-sw}}$ with samples grouped according to $\delta^{18}\text{O}_{\text{con}}$ (where available), comparison between the concretion abundance record and the preservation of marine sedimentary rock, the temporal trend of $\Delta^{13}\text{C}_{\text{con-sw}}$ maxima, mean and minima alongside major evolutionary events, comparison of the temporal trend of $\Delta^{13}\text{C}_{\text{con-sw}}$ maxima, mean and minima with iron speciation data and select reaction transport model results. Supplementary material to this article can be found online at <https://doi.org/10.1016/j.gca.2023.04.022>.

References

- Adams, D.D., Hurtgen, M.T., Sageman, B.B., 2010. Volcanic triggering of a biogeochemical cascade during Oceanic Anoxic Event 2. *Nat. Geosci.* 3 (3), 201–204.
- Algeo, T., Luo, G., Song, H., Lyons, T., Canfield, D., 2015. Reconstruction of secular variation in seawater sulfate concentrations. *Biogeosciences* 12 (7), 2131–2151.
- Aller, R., Blair, N., Xia, Q., Rude, P., 1996. Remineralization rates, recycling, and storage of carbon in Amazon shelf sediments. *Cont. Shelf Res.* 16 (5–6), 753–786.
- Allison, P.A., Pye, K., 1994. Early diagenetic mineralization and fossil preservation in modern carbonate concretions. *Palaios* 9, 561–575.
- Anderson, J.J., Devol, A.H., 1973. Deep water renewal in Saanich Inlet, an intermittently anoxic basin. *Estuar. Coast. Mar. Sci.* 1 (1), 1–10.
- Arndt, S., Jørgensen, B.B., LaRowe, D.E., Middelburg, J., Pancost, R., Regnier, P., 2013. Quantifying the degradation of organic matter in marine sediments: A review and synthesis. *Earth Sci. Rev.* 123, 53–86.
- Bartley, J.K., Kah, L.C., 2004. Marine carbon reservoir, Corg-Ccarb coupling, and the evolution of the Proterozoic carbon cycle. *Geology* 32 (2), 129.
- Battistuzzi, F.U., Feijao, A., Hedges, S.B., 2004. A genomic timescale of prokaryote evolution: insights into the origin of methanogenesis, phototrophy, and the colonization of land. *BMC Evol. Biol.* 4 (1), 44.
- Bekker, A., Holland, H., 2012. Oxygen overshoot and recovery during the early Paleoproterozoic. *Earth Planet. Sci. Lett.* 317, 295–304.
- Berner, R.A., 1980. Early diagenesis: A theoretical approach. Princeton University Press.
- Berner, R.A., 2004. A model for calcium, magnesium and sulfate in seawater over Phanerozoic time. *Am. J. Sci.* 304 (5), 438–453.
- Berner, R.A., Canfield, D.E., 1989. A new model for atmospheric oxygen over Phanerozoic time. *Am. J. Sci.* 289 (4), 333–361.
- Birgel, D., Meister, P., Lundberg, R., Horath, T., Bontognali, T.R., Bahniuk, A.M., de Rezende, C.E., Váscancelos, C., McKenzie, J.A., 2015. Methanogenesis produces strong ^{13}C enrichment in stromatolites of Lagoa Salgada, Brazil: a modern analogue for Palaeo-/Neoproterozoic stromatolites? *Geobiology* 13 (3), 245–266.
- Bjørlykke, K., 1973. Origin of limestone nodules in the Lower Palaeozoic of the Oslo Region. Universitetsforlaget.
- Blättler, C.L., Bergmann, K.D., Kah, L.C., Gómez-Pérez, I., Higgins, J.A., 2020. Constraints on Meso-to Neoproterozoic seawater from ancient evaporite deposits. *Earth Planet. Sci. Lett.* 532, 115951.
- Blättler, C., Claire, M., Prave, A.R., Kirsinmäe, K., Higgins, J., Medvedev, P., Romashkin, A., Rychanchik, D., Zerkle, A.L., Paiste, K., 2018. Two-billion-year-old evaporites capture Earth's great oxidation. *Science* 360 (6386), 320–323.
- Blome, C.D., Albert, N.R., 1985. Carbonate concretions: An ideal sedimentary host for microfossils. *Geology* 13 (3), 212–215.
- Bojanowski, M.J., Barczuk, A., Wetzel, A., 2014. Deep-burial alteration of early-diagenetic carbonate concretions formed in Palaeozoic deep-marine greywackes and mudstones (Bardo Unit, Sudetes Mountains, Poland). *Sedimentology* 61 (5), 1211–1239.
- Bottinga, Y., 1969. Calculated fractionation factors for carbon and hydrogen isotope exchange in the system calcite-carbon dioxide-graphite-methane-hydrogen-water vapor. *Geochim. Cosmochim. Acta* 33 (1), 49–64.
- Botz, R., Pokojski, H.-D., Schmitt, M., Thomm, M., 1996. Carbon isotope fractionation during bacterial methanogenesis by CO_2 reduction. *Org. Geochem.* 25 (3–4), 255–262.
- Bradbury, H.J., Turchyn, A.V., 2019. Reevaluating the carbon sink due to sedimentary carbonate formation in modern marine sediments. *Earth Planet. Sci. Lett.* 519, 40–49.
- Bradley, D.C., 2008. Passive margins through earth history. *Earth Sci. Rev.* 91 (1–4), 1–26.
- Bramlette, M.N., 1946. The Monterey Formation of California and the origin of its siliceous rocks. US Government Printing Office, Washington.
- Bristow, T.F., Grotzinger, J.P., 2013. Sulfate availability and the geological record of cold-seep deposits. *Geology* 41 (7), 811–814.
- Brocks, J.J., Jarrett, A.J., Siraotino, E., Hallmann, C., Hoshino, Y., Liyanage, T., 2017. The rise of algae in Cryogenian oceans and the emergence of animals. *Nature* 548 (7669), 578–581.
- Burdige, D.J., 2005. Burial of terrestrial organic matter in marine sediments: A re-assessment. *Global Biogeochem. Cycles* 19 (4).
- Burdige, D.J., 2007. Preservation of organic matter in marine sediments: controls, mechanisms, and an imbalance in sediment organic carbon budgets? *Chem. Rev.* 107 (2), 467–485.
- Burns, S.J., Baker, P.A., 1987. A geochemical study of dolomite in the Monterey Formation, California. *J. Sediment. Res.* 57 (1).
- Canfield, D., 1998. A new model for Proterozoic ocean chemistry. *Nature* 396 (6710), 450–453.
- Chen, X., Ling, H.-F., Vance, D., Shields-Zhou, G.A., Zhu, M., Poulton, S.W., Och, L.M., Jiang, S.-Y., Li, D., Cremonese, L., 2015. Rise to modern levels of ocean oxygenation coincided with the Cambrian radiation of animals. *Nat. Commun.* 6 (1), 1–7.
- Claypool, G.E., Kaplan, I., 1974. The origin and distribution of methane in marine sediments. *Natural gases in marine sediments*. Springer, New York, pp. 99–139.
- Coleman, M.L., 1993. Microbial processes: controls on the shape and composition of carbonate concretions. *Mar. Geol.* 113 (1–2), 127–140.
- Craddock, P.R., Dauphas, N., 2011. Iron and carbon isotope evidence for microbial iron respiration throughout the Archean. *Earth Planet. Sci. Lett.* 303 (1–2), 121–132.
- Dale, A., John, C.M., Mozley, P.S., Smalley, P., Muggerridge, A.H., 2014. Time-capsule concretions: unlocking burial diagenetic processes in the Mancos Shale using carbonate clumped isotopes. *Earth Planet. Sci. Lett.* 394, 30–37.
- Dehler, C., Elrick, M., Bloch, J., Crossey, L., Karlstrom, K., Marais, D.D., 2005. High-resolution $\delta^{13}\text{C}$ stratigraphy of the Chuar Group (ca. 770–742 Ma), Grand Canyon: Implications for mid-Neoproterozoic climate change. *Geol. Soc. Am. Bull.* 117(1–2), 32–45.
- Derry, L.A., Kaufman, A.J., Jacobsen, S.B., 1992. Sedimentary cycling and environmental change in the Late Proterozoic: evidence from stable and radiogenic isotopes. *Geochim. Cosmochim. Acta* 56 (3), 1317–1329.
- Des Marais, D.J., Strauss, H., Summons, R.E., Hayes, J., 1992. Carbon isotope evidence for the stepwise oxidation of the Proterozoic environment. *Nature* 359 (6396), 605–609.
- Dix, G.R., Thomson, M.L., Longstaffe, F.J., McNutt, R.H., 1995. Systematic decrease of high $\delta^{13}\text{C}$ values with burial in late Archaean (2.8 Ga) diagenetic dolomite: evidence for methanogenesis from the Crixás Greenstone Belt, Brazil. *Precamb. Res.* 70 (3–4), 253–268.
- Duck, R., 1995. Subaqueous shrinkage cracks and early sediment fabrics preserved in Pleistocene calcareous concretions. *J. Geol. Soc. London* 152 (1), 151–156.
- Efron, B., 1979. Bootstrap methods: Another look at the jackknife. *Ann. Stat.* 7, 1–26.
- Efron, B., 1982. The jackknife, the bootstrap and other resampling plans. SIAM, Philadelphia PA.
- Eguchi, J., Seales, J., Dasgupta, R., 2020. Great Oxidation and Lomagundi events linked by deep cycling and enhanced degassing of carbon. *Nat. Geosci.* 13 (1), 71–76.
- El Albani, A., Vachard, D., Kuhnt, W., Thurov, J., 2001. The role of diagenetic carbonate concretions in the preservation of the original sedimentary record. *Sedimentology* 48 (4), 875–886.
- Emrich, K., Ehhalt, D., Vogel, J., 1970. Carbon isotope fractionation during the precipitation of calcium carbonate. *Earth Planet. Sci. Lett.* 8 (5), 363–371.
- Evans, D.A., 2006. Proterozoic low orbital obliquity and axial-dipolar geomagnetic field from evaporite palaeolatitudes. *Nature* 444 (7115), 51–55.
- Fakrae, M., Crowe, S.A., Katsev, S., 2018. Sedimentary sulfur isotopes and Neoproterozoic ocean oxygenation. *Sci. Adv.* 4 (1) e1701835.
- Fakrae, M., Hancisse, O., Canfield, D.E., Crowe, S.A., Katsev, S., 2019. Proterozoic seawater sulfate scarcity and the evolution of ocean-atmosphere chemistry. *Nat. Geosci.* 12 (5), 375–380.
- Gaines, R.R., Kennedy, M.J., Droser, M.L., 2005. A new hypothesis for organic preservation of Burgess Shale taxa in the middle Cambrian Wheeler Formation, House Range, Utah. *Palaeogeogr. Palaeoclimatol. Palaeoecol.* 220 (1–2), 193–205.
- Galimov, E., Kvenvolden, K.A., 1983. Concentrations and carbon isotopic compositions of CH_4 and CO_2 in gas from sediments of the Blake Outer Ridge, Deep Sea Drilling Project Leg 76. Initial Reports of the DSDP 76, 403–407.
- Gibling, M.R., Davies, N.S., 2012. Palaeozoic landscapes shaped by plant evolution. *Nat. Geosci.* 5 (2), 99–105.
- Gill, B.C., Lyons, T.W., Saltzman, M.R., 2007. Parallel, high-resolution carbon and sulfur isotope records of the evolving Paleozoic marine sulfur reservoir. *Palaeogeogr. Palaeoclimatol. Palaeoecol.* 256 (3–4), 156–173.
- Gill, B.C., Lyons, T.W., Young, S.A., Kump, L.R., Knoll, A.H., Saltzman, M.R., 2011. Geochemical evidence for widespread euxinia in the later Cambrian ocean. *Nature* 469 (7328), 80–83.
- Gross, M.G., Tracey Jr, J.L., 1966. Oxygen and carbon isotopic composition of limestones and dolomites, Bikini and Eniwetok Atolls. *Science* 151 (3714), 1082–1084.
- Grotzinger, J.P., James, N.P., 2000. Precambrian carbonates: evolution of understanding. Habicht, K.S., Gade, M., Thamdrup, B., Berg, P., Canfield, D.E., 2002. Calibration of sulfate levels in the Archean ocean. *Science* 298 (5602), 2372–2374.
- Halevy, I., Johnston, D.T., Schrag, D.P., 2010. Explaining the structure of the Archean mass-independent sulfur isotope record. *Science* 329 (5988), 204–207.
- Halevy, I., Peters, S.E., Fischer, W.W., 2012. Sulfate burial constraints on the Phanerozoic sulfur cycle. *Science* 337 (6092), 331–334.
- Halverson, G.P., Hoffman, P.F., Schrag, D.P., Maloof, A.C., Rice, A.H.N., 2005. Toward a Neoproterozoic composite carbon-isotope record. *Geol. Soc. Am. Bull.* 117 (9), 1181.
- Hayes, J.M., Waldbauer, J.R., 2006. The carbon cycle and associated redox processes through time. *Philos. Trans. R. Soc., B* 361 (1470), 931–950.
- Hedges, J.L., Keil, R.G., Benner, R., 1997. What happens to terrestrial organic matter in the ocean? *Org. Geochem.* 27 (5–6), 195–212.
- Heimhofer, U., Meister, P., Bernasconi, S.M., Ariztegui, D., Martill, D.M., Rios-Netto, A.M., Schwark, L., 2017. Isotope and elemental geochemistry of black shale-hosted fossiliferous concretions from the Cretaceous Santana Formation fossil Lagerstätte (Brazil). *Sedimentology* 64 (1), 150–167.
- Hesselbo, S., Palmer, T., 1992. Reworked early diagenetic concretions and the bioerosional origin of a regional discontinuity within British Jurassic marine mudstones. *Sedimentology* 39 (6), 1045–1065.
- Heuer, V.B., Pohlman, J.W., Torres, M.E., Elvert, M., Hinrichs, K.-U., 2009. The stable carbon isotope biogeochemistry of acetate and other dissolved carbon species in deep seafloor sediments at the northern Cascadia Margin. *Geochim. Cosmochim. Acta* 73 (11), 3323–3336.
- Hinrichs, K.U., 2002. Microbial fixation of methane carbon at 2.7 Ga: Was an anaerobic mechanism possible? *Geochem. Geophys. Geosyst.* 3 (7), 1–10.
- Holland, H.D., 2002. Volcanic gases, black smokers, and the Great Oxidation Event. *Geochim. Cosmochim. Acta* 66 (21), 3811–3826.
- Horita, J., 2001. Carbon isotope exchange in the system CO_2 - CH_4 at elevated temperatures. *Geochim. Cosmochim. Acta* 65 (12), 1907–1919.
- Horita, J., Zimmermann, H., Holland, H.D., 2002. Chemical evolution of seawater during the Phanerozoic: Implications from the record of marine evaporites. *Geochim. Cosmochim. Acta* 66 (21), 3733–3756.
- Hurtgen, M.T., Arthur, M.A., Suits, N.S., Kaufman, A.J., 2002. The sulfur isotopic composition of Neoproterozoic seawater sulfate: implications for a snowball Earth? *Earth Planet. Sci. Lett.* 203 (1), 413–429.
- Husson, J.M., Peters, S.E., 2018. Nature of the sedimentary rock record and its implications for Earth system evolution. *Emerging Top. Life Sci.* 2 (2), 125–136.

- Irwin, H., Curtis, C., Coleman, M., 1977. Isotopic evidence for source of diagenetic carbonates formed during burial of organic-rich sediments. *Nature* 269, 209–213.
- Jacobs, L., Emerson, S., Skei, J., 1985. Partitioning and transport of metals across the O₂H₂S interface in a permanently anoxic basin: Framvaren Fjord, Norway. *Geochim. Cosmochim. Acta* 49 (6), 1433–1444.
- Kah, L.C., Lyons, T.W., Frank, T.D., 2004. Low marine sulphate and protracted oxygenation of the Proterozoic biosphere. *Nature* 431 (7010), 834–838.
- Karhu, J.A., Holland, H.D., 1996. Carbon isotopes and the rise of atmospheric oxygen. *Geology* 24 (10), 867–870.
- Keil, R.G., Montluçon, D.B., Prah, F.G., Hedges, J.I., 1994. Sorptive preservation of labile organic matter in marine sediments. *Nature* 370 (6490), 549–552.
- Kennedy, M., Droser, M., Mayer, L.M., Pevear, D., Mrofka, D., 2006. Late Precambrian oxygenation; inception of the clay mineral factory. *Science* 311 (5766), 1446–1449.
- Kennedy, M.J., Pevear, D.R., Hill, R.J., 2002. Mineral surface control of organic carbon in black shale. *Science* 295 (5555), 657–660.
- Kenrick, P., Crane, P.R., 1997. The origin and early evolution of plants on land. *Nature* 389 (6646), 33–39.
- Kipp, M.A., Krissansen-Totton, J., Catling, D.C., 2021. High organic burial efficiency is required to explain mass balance in Earth's early carbon cycle. *Global Biogeochem. Cycles* 35 (2).
- Knauth, L.P., Kennedy, M.J., 2009. The late Precambrian greening of the Earth. *Nature* 460 (7256), 728–732.
- Koyama, T., 1963. Gaseous metabolism in lake sediments and paddy soils and the production of atmospheric methane and hydrogen. *J. Geophys. Res.* 68 (13), 3971–3973.
- Krause, A.J., Mills, B.J., Merdith, A.S., Lenton, T.M., Poulton, S.W., 2022. Extreme variability in atmospheric oxygen levels in the late Precambrian. *Sci. Adv.* 8 (41), eabm8191.
- Krissansen-Totton, J., Kipp, M.A., Catling, D.C., 2021. Carbon cycle inverse modeling suggests large changes in fractional organic burial are consistent with the carbon isotope record and may have contributed to the rise of oxygen. *Geobiology* 19 (4), 342–363.
- Kump, L.R., Arthur, M.A., 1999. Interpreting carbon-isotope excursions: carbonates and organic matter. *Chem. Geol.* 161 (1), 181–198.
- Laakso, T.A., Schrag, D.P., 2020. The role of authigenic carbonate in Neoproterozoic carbon isotope excursions. *Earth Planet. Sci. Lett.* 549, 116534.
- LaFlamme, C., Barré, G., Fiorentini, M.L., Beaudoin, G., Occhipinti, S., Bell, J., 2021. A significant seawater sulfate reservoir at 2.0 Ga determined from multiple sulfur isotope analyses of the Paleoproterozoic Degruasa Cu-Au volcanogenic massive sulfide deposit, Western Australia. *Geochim. Cosmochim. Acta* 295, 178–193.
- Lenton, T.M., Daines, S.J., Mills, B.J., 2018. COPSE reloaded: An improved model of biogeochemical cycling over Phanerozoic time. *Earth Sci. Rev.* 178, 1–28.
- Liu, A.-Q., Tang, D.-J., Shi, X.-Y., Zhou, L.-M., Zhou, X.-Q., Shang, M.-H., Li, Y., Song, H.-Y., 2019. Growth mechanisms and environmental implications of carbonate concretions from the ~1.4 Ga Xiamaling Formation, North China. *J. Palaeogeogr.* 8 (1), 20.
- Londry, K.L., Dawson, K.G., Grover, H.D., Summons, R.E., Bradley, A.S., 2008. Stable carbon isotope fractionation between substrates and products of *Methanosarcina barkeri*. *Org. Geochem.* 39 (5), 608–621.
- Lowenstein, T.K., Hardie, L.A., Timofeeff, M.N., Demicco, R.V., 2003. Secular variation in seawater chemistry and the origin of calcium chloride basinal brines. *Geology* 31 (10), 857–860.
- Loyd, S., Berelson, W., 2016. The modern record of “concretionary” carbonate: Reassessing a discrepancy between modern sediments and the geologic record. *Chem. Geol.* 420, 77–87.
- Loyd, S.J., Corsetti, F.A., Eiler, J.M., Tripati, A.K., 2012. Determining the diagenetic conditions of concretion formation: assessing temperatures and pore waters using clumped isotopes. *J. Sediment. Res.* 82 (12), 1006–1016.
- Loyd, S.J., Smirnov, M.N., 2022. Progressive formation of authigenic carbonate with depth in siliciclastic marine sediments including substantial formation in sediments experiencing methanogenesis. *Chem. Geol.* 594, 120775.
- Luo, G., Kump, L.R., Wang, Y., Tong, J., Arthur, M.A., Yang, H., Huang, J., Yin, H., Xie, S., 2010. Isotopic evidence for an anomalously low oceanic sulfate concentration following end-Permian mass extinction. *Earth Planet. Sci. Lett.* 300 (1–2), 101–111.
- Lyons, T., Reinhard, C., Scott, C., 2009. Redox redux. *Geobiology* 7 (5), 489–494.
- Lyons, T.W., Reinhard, C.T., Planavsky, N.J., 2014. The rise of oxygen in Earth's early ocean and atmosphere. *Nature* 506 (7488), 307–315.
- Maheshwari, A., Sial, A.N., Gaucher, C., Bossi, J., Bekker, A., Ferreira, V.P., Romano, A. W., 2010. Global nature of the Paleoproterozoic Lomagundi carbon isotope excursion: A review of occurrences in Brazil, India, and Uruguay. *Precamb. Res.* 182 (4), 274–299.
- Martill, D., 1988. Preservation of fish in the Cretaceous Santana Formation of Brazil. *Palaeontology* 31 (1), 1–18.
- McCarty, P.L., 1964. The methane fermentation. Principles and applications in aquatic microbiology, 314–343.
- Meister, P., Liu, B., Ferdelman, T.G., Jørgensen, B.B., Khalili, A., 2013. Control of sulphate and methane distributions in marine sediments by organic matter reactivity. *Geochim. Cosmochim. Acta* 104, 183–193.
- Meister, P., Liu, B., Khalili, A., Böttcher, M.E., Jørgensen, B.B., 2019. Factors controlling the carbon isotope composition of dissolved inorganic carbon and methane in marine porewater: An evaluation by reaction-transport modelling. *J. Mar. Syst.* 200, 103227.
- Meister, P., Reyes, C., 2019. The carbon-isotope record of the sub-seafloor biosphere. *Geosciences* 9 (12), 507.
- Melezhik, V.A., Fallick, A.E., 1996. A widespread positive $\delta^{13}\text{C}_{\text{carb}}$ anomaly at around 2.33–2.06 Ga on the Fennoscandian Shield: a paradox? *Terra Nova* 8 (2), 141–157.
- Mozley, P.S., Burns, S.J., 1993. Oxygen and carbon isotopic composition of marine carbonate concretions: an overview. *J. Sediment. Res.* 63 (1), 73–83.
- Och, L.M., Shields-Zhou, G.A., 2012. The Neoproterozoic oxygenation event: environmental perturbations and biogeochemical cycling. *Earth Sci. Rev.* 110 (1–4), 26–57.
- Ohkouchi, N., Kawamura, K., Kajiura, Y., Wada, E., Okada, M., Kanamatsu, T., Taira, A., 1999. Sulfur isotope records around Livello Bonarelli (northern Apennines, Italy) black shale at the Cenomanian-Turonian boundary. *Geology* 27 (6), 535–538.
- Ohmoto, H., Rye, R.O., 1979. Isotopes of sulfur and carbon. *Geochemistry of hydrothermal ore deposits*, 509–567.
- Orphan, V.J., Ussler, W., Naehr, T.H., House, C.H., Hinrichs, K.U., Paull, C.K., 2004. Geological, geochemical, and microbiological heterogeneity of the seafloor around methane vents in the Eel River Basin, offshore California. *Chem. Geol.* 205 (3–4), 265–289.
- Partin, C., Bekker, A., Planavsky, N., Scott, C., Gill, B., Li, C., Podkovyrov, V., Maslov, A., Konhauser, K., Lalonde, S., 2013. Large-scale fluctuations in Precambrian atmospheric and oceanic oxygen levels from the record of U in shales. *Earth Planet. Sci. Lett.* 369, 284–293.
- Paull, C., Lorenson, T., Borowski, W., Ussler Iii, W., Olsen, K., Rodriguez, N., 2000. Isotopic composition of CH₄, CO₂ species, and sedimentary organic matter within samples from the Blake Ridge: Gas source implications. *Proc. Ocean Drilling Program, Initial Reports* 164, 67–78.
- Pisciotto, K.A., Mahoney, J.J., 1981. Authigenic dolomite in Monterey Formation, California, and related rocks from offshore California and Baja California. *AAPG Bull.* 65 (5), 972–973.
- Planavsky, N.J., McGoldrick, P., Scott, C.T., Li, C., Reinhard, C.T., Kelly, A.E., Chu, X., Bekker, A., Love, G.D., Lyons, T.W., 2011. Widespread iron-rich conditions in the mid-Proterozoic ocean. *Nature* 477 (7365), 448–451.
- Planavsky, N.J., Bekker, A., Hofmann, A., Owens, J.D., Lyons, T.W., 2012. Sulfur record of rising and falling marine oxygen and sulfate levels during the Lomagundi event. *PNAS* 109 (45), 18300–18305.
- Planavsky, N.J., Fakraee, M., Bolton, E.W., Reinhard, C.T., Isson, T.T., Zhang, S., Mills, B.J., 2022. On carbon burial and net primary production through Earth's history. *Am. J. Sci.* 322 (3), 413–460.
- Pohlman, J.W., Ruppel, C., Hutchinson, D.R., Downer, R., Coffin, R.B., 2008. Assessing sulfate reduction and methane cycling in a high salinity pore water system in the northern Gulf of Mexico. *Mar. Pet. Geol.* 25 (9), 942–951.
- Pope, M.C., Grotzinger, J.P., 2003. Paleoproterozoic Stark Formation, Athapuscow basin, northwest Canada: Record of cratonic-scale salinity crisis. *J. Sediment. Res.* 73 (2), 280–295.
- Poulton, S., Raiswell, R., 2002. The low-temperature geochemical cycle of iron: from continental fluxes to marine sediment deposition. *Am. J. Sci.* 302 (9), 774–805.
- Poulton, S.W., Fralick, P.W., Canfield, D.E., 2010. Spatial variability in oceanic redox structure 1.8 billion years ago. *Nat. Geosci.* 3(7), 486–490.
- Prave, A., Kirsimäe, K., Lepland, A., Fallick, A., Kreitsmann, T., Deines, Y.E., Romashkin, A., Rychanchik, D., Medvedev, P., Moussavou, M., 2022. The grandest of them all: the Lomagundi-Jatuli Event and Earth's oxygenation. *J. Geol. Soc. London* 179 (1).
- Price, N., Calvert, S., 1973. The geochemistry of iodine in oxidised and reduced recent marine sediments. *Geochim. Cosmochim. Acta* 37 (9), 2149–2158.
- Raiswell, R., 1971. The growth of Cambrian and Liassic concretions. *Sedimentology* 17 (3–4), 147–171.
- Raiswell, R., Berner, R.A., 1986. Pyrite and organic matter in Phanerozoic normal marine shales. *Geochim. Cosmochim. Acta* 50 (9), 1967–1976.
- Raiswell, R., Canfield, D.E., 1998. Sources of iron for pyrite formation in marine sediments. *Am. J. Sci.* 298 (3), 219–245.
- Ronov, A., Khain, V., Balukhovskiy, A., Seslavinsky, K., 1980. Quantitative analysis of Phanerozoic sedimentation. *Sed. Geol.* 25 (4), 311–325.
- Sackett, W.M., Poag, C.W., Eadie, B.J., 1974. Kerogen recycling in the Ross sea, Antarctica. *Science* 185 (4156), 1045–1047.
- Sahoo, S.K., Planavsky, N.J., Kendall, B., Wang, X., Shi, X., Scott, C., Anbar, A.D., Lyons, T.W., Jiang, G., 2012. Ocean oxygenation in the wake of the Marinoan glaciation. *Nature* 489 (7417), 546–549.
- Salop, L., 1982. *Geologic Development of the Earth in Precambrian*. Nedra, Leningrad, 343.
- Savrdá, C.E., Bottjer, D.J., 1988. Limestone concretion growth documented by trace-fossil relations. *Geology* 16 (10), 908–911.
- Schidlowski, M., Eichmann, R., Junge, C.E., 1975. Precambrian sedimentary carbonates: carbon and oxygen isotope geochemistry and implications for the terrestrial oxygen budget. *Precamb. Res.* 2 (1), 1–69.
- Schidlowski, M., Eichmann, R., Junge, C.E., 1976. Carbon isotope geochemistry of the Precambrian Lomagundi carbonate province, Rhodesia. *Geochim. Cosmochim. Acta* 40 (4), 449–455.
- Schlünz, B., Schneider, R.R., 2000. Transport of terrestrial organic carbon to the oceans by rivers: re-estimating flux-and burial rates. *Int. J. Earth Sci.* 88 (4), 599–606.
- Schrag, D.P., Higgins, J.A., Macdonald, F.A., Johnston, D.T., 2013. Authigenic carbonate and the history of the global carbon cycle. *Science* 339 (6119), 540–543.
- Schröder, S., Bekker, A., Beukes, N., Strauss, H., Van Niekerk, H., 2008. Rise in seawater sulphate concentration associated with the Paleoproterozoic positive carbon isotope excursion: evidence from sulphate evaporites in the ~ 2.2–2.1 Gyr shallow-marine Lucknow Formation, South Africa. *Terra Nova* 20 (2), 108–117.
- Scotchman, I., 1991. The geochemistry of concretions from the Kimmeridge Clay Formation of southern and eastern England. *Sedimentology* 38 (1), 79–106.

- Scott, C., Lyons, T., Bekker, A., Shen, Y.-A., Poulton, S., Chu, X.-L., Anbar, A., 2008. Tracing the stepwise oxygenation of the Proterozoic ocean. *Nature* 452 (7186), 456–459.
- Seewald, J.S., 2003. Organic–inorganic interactions in petroleum-producing sedimentary basins. *Nature* 426 (6964), 327–333.
- Shi, W., Mills, B.J., Li, C., Poulton, S.W., Krause, A.J., He, T., Zhou, Y., Cheng, M., Shields, G.A., 2022. Decoupled oxygenation of the Ediacaran ocean and atmosphere during the rise of early animals. *Earth Planet. Sci. Lett.* 591, 117619.
- Sivan, O., Schrag, D., Murray, R., 2007. Rates of methanogenesis and methanotrophy in deep-sea sediments. *Geobiology* 5 (2), 141–151.
- Skei, J., 1983. Permanently Anoxic Marine Basins: Exchange of Substances across Boundaries. *Ecol. Bull.* 419–429.
- Song, H., Tong, J., Algeo, T.J., Song, H., Qiu, H., Zhu, Y., Tian, L., Bates, S., Lyons, T.W., Luo, G., 2014. Early Triassic seawater sulfate drawdown. *Geochim. Cosmochim. Acta* 128, 95–113.
- Sperling, E.A., Stockey, R.G., 2018. The temporal and environmental context of early animal evolution: Considering all the ingredients of an “explosion”. *Integr. Comp. Biol.* 58 (4), 605–622.
- Sperling, E.A., Wolock, C.J., Morgan, A.S., Gill, B.C., Kunzmann, M., Halverson, G.P., Macdonald, F.A., Knoll, A.H., Johnston, D.T., 2015. Statistical analysis of iron geochemical data suggests limited late Proterozoic oxygenation. *Nature* 523 (7561), 451–454.
- Sunagawa, I., 1994. Nucleation, growth and dissolution of crystals during sedimentogenesis and diagenesis, *Developments in Sedimentology*. Elsevier, pp. 19–47.
- Tosca, N.J., Johnston, D.T., Mushegian, A., Rothman, D.H., Summons, R.E., Knoll, A.H., 2010. Clay mineralogy, organic carbon burial, and redox evolution in Proterozoic oceans. *Geochim. Cosmochim. Acta* 74 (5), 1579–1592.
- Veizer, J., Ala, D., Azmy, K., Bruckschen, P., Buhl, D., Bruhn, F., Carden, G.A., Diener, A., Ebner, S., Godderis, Y., 1999. 87Sr/86Sr, $\delta^{13}\text{C}$ and $\delta^{18}\text{O}$ evolution of Phanerozoic seawater. *Chem. Geol.* 161 (1), 59–88.
- Whiticar, M.J., 1999. Carbon and hydrogen isotope systematics of bacterial formation and oxidation of methane. *Chem. Geol.* 161 (1), 291–314.
- Whiticar, M.J., Faber, E., Schoell, M., 1986. Biogenic methane formation in marine and freshwater environments: CO₂ reduction vs. acetate fermentation— isotope evidence. *Geochim. Cosmochim. Acta* 50 (5), 693–709.
- Wortmann, U.G., Chernyavsky, B.M., 2007. Effect of evaporite deposition on Early Cretaceous carbon and sulphur cycling. *Nature* 446 (7136), 654–656.
- Yoshida, H., Ujihara, A., Minami, M., Asahara, Y., Katsuta, N., Yamamoto, K., Sirono, S.-I., Maruyama, I., Nishimoto, S., Metcalfe, R., 2015. Early post-mortem formation of carbonate concretions around tusk-shells over week-month timescales. *Sci. Rep.* 5, 1–7.
- Yoshinaga, M.Y., Holler, T., Goldhammer, T., Wegener, G., Pohlman, J.W., Brunner, B., Kuypers, M.M., Hinrichs, K.-U., Elvert, M., 2014. Carbon isotope equilibration during sulphate-limited anaerobic oxidation of methane. *Nat. Geosci.* 7 (3), 190–194.
- Zeebe, R.E., 2007. Modeling CO₂ chemistry, $\delta^{13}\text{C}$, and oxidation of organic carbon and methane in sediment porewater: Implications for paleo-proxies in benthic foraminifera. *Geochim. Cosmochim. Acta* 71 (13), 3238–3256.